NACA TN 2684

NATIONAL ADVISORY COMMITTEE FOR AERONAUTICS

TECHNICAL NOTE 2684

A LOW-SPEED INVESTIGATION OF A FUSELAGE-SIDE AIR INLET FOR USE AT TRANSONIC FLIGHT SPEEDS

By Mark R. Nichols and Edwin B. Goral

Langley Aeronautical Laboratory
Langley Field, Va.

Washington
April 1952

NATIONAL ADVISORY COMMITTEE FOR AERONAUTICS

TECHNICAL NOTE 2684

A LOW-SPEED INVESTIGATION OF A FUSELAGE-SIDE AIR INLET FOR USE AT TRANSONIC FLIGHT SPEEDS[1]

By Mark R. Nichols and Edwin B. Goral

SUMMARY

A low-speed investigation in the Langley propeller-research tunnel of annular air inlets designed to avoid compression shocks and attendant boundary-layer separation on the fuselage ahead of the inlets at transonic flight speeds by maintaining substream flow velocities on the fuselage nose was reported in NACA TN 2685. In the present investigation, one of the original annular inlets was converted by the installation of a canopy and a nose-wheel fairing into a twin side inlet in order to study problems involved in applying such an inlet to a fighter airplane. Extensive measurements of pressures on the surface of the model and surveys of the internal flow were conducted at angles of attack of 0°, 3°, and 6° over a wide range of inlet-velocity ratio.

The results of the investigation indicate that the previously tested basic annular inlet can be applied successfully to a side-inlet configuration for a transonic airplane. It appears that, in order to maintain minimum surface velocities ahead of the inlet on the canopy and nose-wheel fairing, these bodies should be approximately triangular at all horizontal sections ahead of the inlet, continue expanding for a short distance back of the inlet, and intersect both the fuselage nose and the inlet lip at right angles.

Separation of the internal flow from the original inlet lip at the higher values of inlet-velocity ratio was eliminated by a thick internal fairing at the expense of some reduction in critical Mach number. A compromise between this inner-lip shape and the original may be desirable.

Pressure recoveries of from 92 to 96 percent of the free-stream dynamic pressure were obtained in the diffuser (after 17-percent area expansion) over the ranges of angle of attack and inlet-velocity ratio useful for high-speed and cruising flight.

---

[1]Supersedes the recently declassified NACA RM L7A06 entitled "A Low-Speed Investigation of a Fuselage-Side Air Inlet for Use at Transonic Flight Speeds" by Mark R. Nichols and Edwin B. Goral, 1947.

INTRODUCTION

A low-speed investigation of annular air inlets designed to maintain substream flow velocities on the fuselage ahead of the inlet for the ranges of angle of attack and inlet-velocity ratio useful for high-speed flight was reported in reference 1. Because of the compression shock which will occur at the point of the nose at slightly supersonic Mach numbers, it appears that subsonic flow will be maintained and boundary-layer separation due to compression shocks will be avoided on the fuselage nose ahead of the inlet of such configurations up to a flight Mach number of about 1.2. Unstable inlet flow and large losses in ram therefore can be avoided and the inlet lip can operate essentially in subsonic flow through the transonic-flight region.

The present investigation was undertaken to study some of the additional problems involved in the design of a fuselage-side transonic air inlet for a single-engine fighter airplane. Because of the difficulty of detailed transonic testing at adequate Reynolds numbers, the tests were conducted in the low-speed Langley propeller-research tunnel. Obviously, many significant phenomena associated with compressibility were not observed; however, the data obtained were considered to afford a useful indication of the basic characteristics and design requirements for such inlets.

For the present tests, the original curved-nose basic inlet of reference 1 was converted by the installation of a canopy and a nose-wheel fairing to an approximately 0.55-scale model of a twin side inlet applicable to a transonic airplane powered by an axial-flow jet-propulsion engine rated at 4000-pounds static thrust at sea level. The area of the inlet was selected to give an inlet-velocity ratio of 0.60 for a flight Mach number of 1.0 at an altitude of 35,000 feet. Both the canopy and the nose-wheel fairing were constructed with wedge-shaped plan forms in an attempt to maintain substream velocities on these components in the same manner that such was accomplished with the basic nose. Curved sides were used on the canopy as contrasted to straight radial sides for the cross sections of the nose-wheel fairing in order to provide different types of intersections and to obtain some information as to the effects of varying the shape of such components. The inner fairing of the original inlet lip (reference 1) was revised for the tests in an attempt to eliminate the flow separation from this surface at the higher values of inlet-velocity ratio. A revised diffuser which expanded the duct area to 117 percent of the inlet area was installed in order to permit a more complete study of the pressure-recovery characteristics of the inlet; this expansion comprises about 60 percent of that required for the type of power plant considered.

The investigation consists of studies of the pressures measured on the surface of the model and in the internal flow for angles of attack of 0°, 3°, and 6° for seven values of inlet-velocity ratio ranging between 0.60 and 1.65.

SYMBOLS

H	total pressure, pounds per square foot
M_{cr}	predicted critical Mach number
p	static pressure, pounds per square foot
p_o	static pressure of free stream, pounds per square foot
q_o	dynamic pressure of free stream, pounds per square foot
V_i	average velocity of flow at inlet, feet per second
V_o	velocity of free stream, feet per second
α	angle of attack of center line of model, degrees

MODEL AND TESTS

A general view of the model and detail views of the inlet are presented as figures 1 and 2, respectively. A line drawing of the nose section of the model is shown in figure 3; corresponding coordinates are given in table I.

The internal-flow system (fig. 4) included an axial-flow fan which was necessary to obtain the higher inlet-velocity ratios. Control of the flow quantity was obtained by varying the speed of the fan motor and the position of the butterfly shutters. The quantity of internal flow was measured by means of the total- and static-pressure tubes at the throat of the venturi and checked by the rake at the exit; a thermocouple attached to the exit rake was used to measure the temperature rise through the fan. Prior to the tunnel tests the venturi was carefully calibrated with and without the fan installed to insure the accuracy of the measurements of the internal-flow quantities. Accurate measurements were obtained so long as fan operation did not introduce rotation in the flow through the venturi. Such rotation could be avoided for any desired quantity of internal flow by simultaneous adjustment of the resistance of the system (by means of the shutters)

and the rotational speed of the fan. In the tunnel tests, uniform nonrotational flow in the venturi throat was obtained for each test condition by adjusting the shutter position and the fan speed until the static-pressure distribution across the venturi throat was uniform. Visual observation of a multitube manometer was used to establish this uniformity.

Surface pressures were measured by means of 257 surface orifices located principally on the right halves of the nose, diffuser, canopy, nose-wheel fairing, and inlet lip as shown in figure 2(a). Inlet pressure surveys were made by means of 40 total-pressure tubes (see fig. 2(c)), three static-pressure tubes, and eight surface orifices located at station 0.3 in the left half of the inlet. Pressures at station 12.6 in the right half of the diffuser were measured by means of 56 total-pressure tubes, five static-pressure tubes, and 11 surface orifices. A rake of four total-pressure tubes at station 1.0 on the inside of the inlet lip 45° from the top of the model was used to detect flow separation from the inside of the lip. A rake of nine total-pressure tubes at station 12.6 on the outside of the lip 45° from the top of the model was used to investigate the boundary layer at the rear of the inlet lip. The locations of pertinent pressure-measuring instrumentation are shown in each figure containing basic data. All pressures were recorded by photographing a multitube manometer.

Pressure surveys were conducted at angles of attack of 0°, 3°, and 6° at seven inlet-velocity ratios ranging between 0.60 and 1.65. A tunnel speed of 100 miles per hour, which corresponds to a Mach number of 0.13 and a Reynolds number of about 2×10^6 based on the maximum cowling diameter, was used for tests at inlet-velocity ratios less than 1.1. The tunnel speed was reduced to 70 miles per hour for the remaining tests in order to obtain the higher values of inlet-velocity ratio with the available blower power.

RESULTS AND DISCUSSION

Nose and inner surface of diffuser.- Static-pressure distributions over the nose and the inner surface of the diffuser at the horizontal center line of the model are presented in figure 5. At an angle of attack of 0°, the velocities in this region were substream (that is, the pressure coefficients were positive) at inlet-velocity ratios of the order of 1.0 and less. As was the case with the basic inlet (reference 1) minimum pressures occurred about 0.8 cowling diameter ahead of the inlet at the lower-inlet-velocity ratios; a second and more negative surface pressure occurred just inside the inlet at inlet-velocity ratios above unity. (See comparison, fig. 6.) The chief effect of increasing

the angle of attack was to increase the velocities on the side of the nose. As the velocities at the side of the nose became superstream at a small angle of attack and as even those for $\alpha = 0^\circ$ would become supersonic at slightly supersonic flight Mach numbers, it appears that the curvature in the side should be reduced to assure the avoidance of shock formation. Data presented in reference 1 indicate that the pressure coefficient at this critical section can be made more positive by an increment of about 0.06 through the use of a straight-sided conical nose of the same length.

A comparison of the static-pressure distributions over the top of the model (fig. 7) with those for the basic nose (fig. 6) shows that the addition of the canopy caused general decreases in the flow velocity at the top of the nose, especially in the critical region 0.8 cowling diameter ahead of the inlet. Substream velocities were maintained over the ranges of inlet-velocity ratio and angle of attack useful for high-speed flight. Substream velocities at the bottom of the nose also would be anticipated for this flight region because of a similar favorable influence of the nose-wheel fairing. Increasing the angle of attack decreased the local velocities in the top of the inlet and increased those at the bottom, as was the case with the basic inlet of reference 1.

Static-pressure distributions in the intersection of the nose and inner surface of the diffuser with the canopy and the nose-wheel fairing are shown in figures 8 and 9, respectively. At an angle of attack of 0°, the peak velocities in these intersections were somewhat higher than those for corresponding stations on the side of the nose and diffuser (fig. 5) but remained less than the free-stream value for the high-speed range of inlet-velocity ratio. Increases in the angle of attack caused small decreases in the velocities in the canopy intersection and small noncritical increases in the velocities in the nose-wheel-fairing intersection. These results indicate that the design of intersections for such fairings in the top or bottom of this type of inlet presents no special problem provided that the fairing is approximately triangular in plan form and continues expanding for a short distance inside the inlet.

Canopy.- Static-pressure distributions on the basic canopy contours (fig. 3) are shown in figure 10. At an angle of attack of 0° and inlet-velocity ratios of 0.90 and less, substream velocities were maintained inside and forward of the inlet for all water lines except 12 and 13 which were well above the inlet. For a typical high-speed condition, $\alpha = 0^\circ$ and $\frac{V_i}{V_o} = 0.71$, the maximum negative pressure coefficient measured on the canopy contours above and behind the inlet was -0.31, a value corresponding to a critical Mach number of 0.77 as predicted

according to the von Kármán relationship (reference 2). The main effect on the canopy contours of increasing the angle of attack was, in general, to decrease the negative peak pressures on the contours below the intersection with the inlet lip by a small amount and to cause small increases in those for the contours above this intersection.

Static-pressure distributions in the intersection of the canopy with the inlet lip are given in figure 11. Substream velocities were maintained in the internal flow at all angles of attack for inlet-velocity ratios of 0.90 and less. Further discussion of these data is contained in succeeding sections entitled "Inlet-lip intersections" and "Minimum surface pressures and critical Mach numbers."

Nose-wheel fairing.- Static-pressure distributions on the bottom and side of the nose-wheel fairing (fig. 3) are presented in figure 12. The velocities on the side of the fairing were substream at an angle of attack of 0° for inlet-velocity ratios of 0.90 and below. Superstream velocities, however, occurred on the bottom edges of this fairing in the vicinity of the inlet for these conditions, and the steep pressure gradients along the edge indicate a pronounced flow around the corner. A vee-bottomed fairing similar to the canopy, in which each horizontal section is approximately wedge-shaped, therefore may be preferable to the present bottom.

Static-pressure distributions in the intersection of the nose-wheel fairing with the inlet lip (fig. 13) show that substream velocities were maintained on the internal-lip surface for the ranges of inlet-velocity ratio and angle of attack useful for high-speed flight. Data presented in the succeeding section of the paper entitled "Inlet-lip intersections" show that the pressure distributions in this intersection were essentially similar to those over isolated parts of the inlet lip.

Inlet lip.- Surface-pressure distributions around the nose of the inlet lip at the horizontal center line of the model (fig. 14) show that velocities on the inner surface of the lip were substream for the usual high-speed range of inlet-velocity ratio and that the surface pressures at this section of the lip were insensitive to moderate changes in angle of attack. Furthermore, boundary-layer surveys in the internal and external flow (figs. 15 and 16, respectively) indicate that the flow did not separate from either surface of the inlet lip over the complete test ranges of angle of attack and inlet-velocity ratio.

The NACA 1-85-050 cowling (reference 3) used as the basic inlet was modified for the present tests by the addition of a thick inner-lip fairing in an attempt to eliminate the internal separation noted in reference 1. Pressure distributions over the lip with and without this

revision are shown in figure 17. At the higher inlet-velocity ratios, use of the revised fairing caused large reductions in the negative pressure peaks on the inside of the lip and, as shown in figure 15, gave no evidence of separation. At the lower values of inlet-velocity ratio which correspond to high-speed flight, however, the change in lip shape caused an appreciable increase in the negative pressures over the external surface of the lip. At $\frac{V_i}{V_o} = 0.80$, for example, the predicted critical Mach number for the revised lip was 0.73 as compared with 0.78 for the lip of the original inlet. This result indicates that the best inner-lip shape is perhaps a compromise between the revised fairing and the original fairing.

Inlet-lip intersections.- A comparison of the static-pressure distributions over several sections of the inlet lip is presented in figure 18. The velocities in the external intersections of the lip with the canopy and the nose-wheel fairing were higher and slightly lower, respectively, than those at the horizontal center line of the model because of the shapes of the respective fairings. The stagnation point on the lip at the intersection of the lip with the canopy also was displaced toward the inside of the inlet due to the slope of the canopy at the intersection; at the same time, the negative pressure peak in the external part of the intersection increased in value and moved forward. Such a distortion of the pressure distribution did not occur in the intersection of the lip with the nose-wheel fairing. These results indicate the advantages obtained by the use of right-angular intersections.

Minimum surface pressures and critical Mach numbers.- The minimum surface pressures measured on the model for $\alpha = 0^\circ$ and corresponding critical Mach numbers predicted according to reference 2 are summarized in figure 19. These data show that the present design achieved the desired primary objective of maintaining substream velocities on the surfaces in front of the inlet for the inlet-velocity ratios useful for high-speed flight, except at the edge of the nose-wheel fairing. At higher angles of attack the velocities on the side of the nose also became superstream. Adequate reductions in the velocities at these critical points appear to be obtainable by replacing the present nose-wheel fairing with a vee-bottomed fairing similar to the canopy and by making the nose a straight-sided cone (as was described in reference 1).

It appears that the critical speed of the intersection of the inlet lip with the canopy can be increased and superstream velocities at the front of this intersection avoided by broadening the canopy above the nose of the inlet lip to obtain a more nearly rectangular intersection, and by making the contours of the canopy approximately

triangular at all horizontal sections ahead of the inlet to keep the velocities low on the sides of the canopy. The latter modification also would reduce or eliminate the superstream velocities on the forward part of canopy water lines 12 and 13. As is the case with the present inlet, the canopy contours must continue expanding for a short distance back of the inlet to avoid local increments of velocity at the inlet due to excessive surface curvature.

Means for increasing the critical speed of the inlet lip were not investigated in the present tests as results presented in reference 1 indicate that satisfactory lips for this type of inlet can be designed by application of existing data for the NACA 1-series nose inlets. The design charts of reference 3 cover the selection of the NACA 1-series inlets for critical Mach numbers approaching 0.9.

Pressure surveys in inlet.- Pressure surveys at measuring station 0.3 in the inlet are shown in figure 20. At an angle of attack of 0° a pressure-recovery coefficient of unity was obtained over most of the inlet for all inlet-velocity ratios, and the entering boundary layers were comparatively thin even in the corners of the inlet. The effect of increasing the angle of attack was to cause small regions of pressure loss at the top and bottom of the inlet. The indicated losses at the top of the inlet, which were especially severe at the lower values of inlet-velocity ratio, are attributed, in part, to the thickening of the boundary layer on the top of the nose (see reference 1) and possibly also to the angularity of flow at the measuring tubes. The losses at the bottom of the inlet, which were significant only at the highest values of inlet-velocity ratio, are believed to have been caused by separation of the flow from the edge of the nose-wheel fairing.

Pressure surveys in diffuser.- Pressure surveys at station 12.6 in the diffuser (after about 17-percent area expansion) are shown in figure 21. Pressure-recovery coefficients of unity still were obtained in the central parts of the duct at all angles of attack and all inlet-velocity ratios. The boundary layers on the walls, however, were much thicker than those at the inlet and large pressure losses were measured in the vicinity of the intersection of the canopy with the inner surface of the diffuser, especially at the lower inlet-velocity ratios at the higher angles of attack. At $\alpha = 6^\circ$ and $\frac{V_i}{V_o} = 0.60$, very little flow passed through the top quarter of the inlet.

The integrated average of the total-pressure recoveries at station 12.6 in the diffuser is presented in figure 22 as a function of inlet-velocity ratio for angles of attack of 0°, 3°, and 6°. Pressure recoveries of from $0.92q_o$ to $0.96q_o$ were obtained at this station over

the ranges of angle of attack and inlet-velocity ratio useful for high-speed and cruising flight.

SUMMARY OF RESULTS

A low-speed investigation was made of a fuselage-side air inlet designed to operate at transonic flight speeds. This inlet was obtained by adding a canopy and a nose-wheel fairing to one of the basic annular inlets of NACA TN 2685. The more significant results and conclusions of the investigation are summarized as follows:

1. The required substream velocities were maintained on the surfaces in front of the inlets for the inlet-velocity ratios useful for high-speed flight except at the edge of the nose-wheel fairing. At higher angles of attack the velocities at the side of the nose also became superstream. Adequate reductions in the velocities at these critical points can be obtained by replacing the present nose-wheel fairing with a vee-bottomed fairing similar to the canopy and by making the nose a straighted-sided cone.

2. It appears that in order to maintain minimum surface velocities ahead of the inlet on the canopy and nose-wheel fairing, these bodies should be approximately triangular at all horizontal sections ahead of the inlet, continue expanding for a short distance back of the inlet, and intersect both the fuselage nose and the inlet lip at right angles.

3. Separation of the internal flow from the original inlet lip at the higher values of inlet-velocity ratio was eliminated by a thick internal fairing at the expense of some reduction in critical Mach number. A compromise between this inner-lip shape and the original may be desirable.

4. Pressure recoveries of from 92 to 96 percent of the free-stream dynamic pressure were obtained in the diffuser (after 17-percent area expansion) over the ranges of angle of attack and inlet-velocity ratio useful for high-speed and cruising flight.

Langley Aeronautical Laboratory
National Advisory Committee for Aeronautics
Langley Field, Va., January 24, 1947

REFERENCES

1. Nichols, Mark R., and Rinkoski, Donald W.: A Low-Speed Investigation of an Annular Transonic Air Inlet. NACA TN 2685, 1952. (Supersedes NACA RM L6J04.)

2. Von Kármán, Th.: Compressibility Effects in Aerodynamics. Jour. Aero. Sci., vol. 8, no. 9, July 1941, pp. 337-356.

3. Baals, Donald D., Smith, Norman F., and Wright, John B.: The Development and Application of High-Critical-Speed Nose Inlets. NACA Rep. 920, 1948. (Supersedes NACA ACR L5F30a.)

TABLE I.- COORDINATES OF NOSE SECTION OF MODEL

[See fig. 3 for identification of symbols; all dimensions are in inches]

Nose	
X	R_N
-54.00	0
-52.00	.57
-50.00	1.09
-47.50	1.69
-45.00	2.29
-40.00	3.42
-35.00	4.49
-30.00	5.47
-25.00	6.33
-20.00	7.07
-15.00	7.71
-10.00	8.23
-5.00	8.70
-2.50	8.90
0	9.10

Top of canopy					
X	WL	X	WL	X	WL
-15.00	7.30	0	14.23	21.00	15.40
-14.00	8.59	1.00	14.47	22.00	15.32
-13.00	9.20	2.00	14.68	23.00	15.22
-12.00	9.82	3.00	14.89	24.00	15.17
-11.00	10.32	4.00	15.08	25.00	15.04
-10.00	10.78	5.00	15.24	26.00	14.99
-9.00	11.21	6.00	15.37	27.00	14.86
-8.00	11.63	7.00	15.46	28.00	14.79
-7.00	12.04	8.00	15.56	29.00	14.69
-6.00	12.42	9.00	15.64	30.00	14.60
-5.00	12.79	10.00	15.72	31.00	14.50
-4.00	13.11	11.00	15.78	32.00	14.40
-3.00	13.42	12.00	15.79	33.00	14.31
-2.00	13.70	13.00	15.80	34.00	14.21
-1.00	13.98	14.00	15.79	35.00	14.12
		15.00	15.78	36.00	14.01
		16.00	15.76	37.00	13.92
		17.00	15.70	38.00	13.80
		18.00	15.62	39.00	13.72
		19.00	15.58	40.00	13.62
		20.00	15.49	-----	-----

TABLE I.- COORDINATES OF NOSE SECTION OF MODEL - Continued.

Nose-wheel fairing						
X	Z					R_W
	WL 9	WL 10	WL 11	WL 12	WL 13	
-10.15	----	----	----	----	----	8.25
-10.00	0.06	----	----	----	----	8.41
-9.00	.37	0.41	----	----	----	9.21
-8.00	.61	.68	----	----	----	9.84
-7.00	.82	.91	----	----	----	10.27
-6.00	1.02	1.13	1.24	----	----	10.70
-5.00	1.20	1.33	1.47	----	----	11.03
-4.00	1.37	1.52	1.67	----	----	11.38
-3.00	1.50	1.66	1.83	----	----	11.65
-2.00	1.62	1.80	1.98	2.16	----	11.88
-1.00	1.74	1.93	2.12	2.32	----	12.14
0	1.84	2.05	2.26	2.46	----	12.33
1.00	1.92	2.15	2.35	2.56	----	12.53
2.00	2.01	2.23	2.46	2.67	----	12.71
3.00	2.07	2.30	2.54	2.76	----	12.86
4.00	2.13	2.36	2.60	2.84	3.07	13.00
5.00	2.18	2.42	2.67	2.91	3.15	13.11
6.00	2.22	2.47	2.72	2.97	3.22	13.21
7.00	2.27	2.52	2.78	3.03	3.28	13.31
8.00	2.31	2.57	2.83	3.08	3.34	13.40
9.00	2.34	2.61	2.87	3.13	3.39	13.48
10.00	2.37	2.63	2.89	3.16	3.42	13.51
11.00	2.38	2.64	2.91	3.17	3.43	13.58
12.00	2.39	2.65	2.92	3.19	3.45	13.60
13.00	2.39	2.65	2.92	3.19	3.45	13.61
13.62	2.39	2.65	2.92	3.19	3.45	13.62

TABLE I.- COORDINATES OF NOSE SECTION OF MODEL - Continued.

Canopy water lines								
X	Y_C							
	WL 15	WL 14	WL 13	WL 12	WL 11	WL 10	WL 9	WL 8
-15.80	----	----	----	----	----	----	----	0
-15.00	----	----	----	----	----	----	----	.10
-14.00	----	----	----	----	----	----	----	.40
-13.35	----	----	----	----	----	----	0	----
-13.00	----	----	----	----	----	----	.19	.80
-12.00	----	----	----	----	----	----	.70	1.15
-11.64	----	----	----	----	----	0	----	----
-11.00	----	----	----	----	----	.45	1.15	1.45
-10.00	----	----	----	----	----	1.08	1.59	1.77
-9.47	----	----	----	----	0	----	----	----
-9.00	----	----	----	----	.58	1.67	2.02	----
-8.00	----	----	----	----	1.44	2.18	2.40	----
-7.10	----	----	----	0	----	----	----	----
-7.00	----	----	----	----	2.12	2.65	2.80	----
-6.00	----	----	----	1.36	2.69	3.08	3.15	----
-5.00	----	----	----	2.12	3.20	3.55	3.50	----
-4.32	----	----	0	----	----	----	----	----
-4.00	----	----	.72	2.72	3.64	3.82	3.80	----
-3.00	----	----	1.92	3.34	4.06	4.18	4.05	----
-2.00	----	----	2.53	3.72	4.38	4.47	4.35	----
-1.00	----	----	3.04	4.08	4.69	4.73	4.54	----
-.94	----	0	----	----	----	----	----	----
0	----	1.58	3.48	4.40	4.98	5.05	4.70	----
1.00	----	2.25	3.85	4.68	5.23	5.25	4.85	4.25
2.00	----	2.74	4.21	4.94	5.38	5.42	4.98	4.38
3.00	----	3.16	4.45	5.18	5.45	5.56	5.09	4.50
3.57	0	----	----	----	----	----	----	----
4.00	1.00	3.52	4.68	5.41	----	5.67	5.18	4.60
5.00	1.73	3.80	4.88	5.59	----	5.76	5.27	4.68
6.00	2.17	4.01	5.05	5.74	----	5.82	5.34	4.76
7.00	2.45	4.17	5.20	5.85	----	5.87	5.40	4.82
8.00	2.70	4.33	5.31	5.96	----	5.92	5.46	4.88
9.00	2.88	4.44	5.40	6.05	----	5.96	5.51	4.94
10.00	3.08	4.57	5.50	6.14	----	5.98	5.55	4.97
11.00	3.21	4.66	5.58	6.21	----	6.00	5.57	4.99
12.00	3.26	4.70	5.60	6.23	----	6.00	5.59	5.00
13.00	3.26	4.70	5.60	6.23	----	6.00	5.60	5.00
13.62	----	----	----	----	----	6.00	5.60	5.00
14.00	3.26	4.70	5.60	6.23	----	----	----	----
15.00	3.21	4.66	5.58	6.21	----	----	----	----
16.00	3.18	4.64	5.56	6.19	----	----	----	----
17.00	3.03	4.55	5.48	----	----	----	----	----
18.00	2.88	4.41	5.37	----	----	----	----	----
19.00	2.74	4.35	5.32	----	----	----	----	----
20.00	2.49	4.20	5.20	----	----	----	----	----
21.00	2.26	4.06	5.09	----	----	----	----	----
22.00	2.00	3.92	4.98	----	----	----	----	----
23.00	1.61	3.77	4.86	----	----	----	----	----
24.00	1.30	3.69	4.80	----	----	----	----	----
25.00	.75	3.44	4.62	----	----	----	----	----
25.60	0	----	----	----	----	----	----	----
26.00	----	3.35	4.55	----	----	----	----	----
27.00	----	3.12	4.37	----	----	----	----	----
28.00	----	2.90	4.26	----	----	----	----	----
29.00	----	2.76	4.12	----	----	----	----	----
30.00	----	2.57	4.00	----	----	----	----	----
31.00	----	2.32	----	----	----	----	----	----
32.00	----	2.10	----	----	----	----	----	----
33.00	----	1.82	----	----	----	----	----	----
34.00	----	1.58	----	----	----	----	----	----
35.00	----	1.18	----	----	----	----	----	----
36.00	----	.03	----	----	----	----	----	----
36.10	----	0	----	----	----	----	----	----

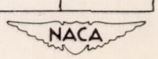

TABLE I.- COORDINATES OF NOSE SECTION OF MODEL - Concluded.

Inlet lip			
External surface		Internal surface	
X	Y	X'	Y'
0	0	0	0
.03	.10	.008	.029
.08	.16	.016	.041
.14	.21	.033	.060
.20	.25	.049	.075
.27	.29	.07	.09
.41	.36	.08	.10
.54	.43	.12	.13
.68	.49	.16	.15
.82	.54	.25	.18
.95	.59	.33	.21
1.09	.63	.41	.23
1.23	.68	.49	.25
1.36	.72	.57	.26
1.70	.82	.65	.27
2.04	.90	.74	.28
2.38	.98	.82	.28
2.72	1.05		
3.41	1.18		
4.09	1.29		
4.77	1.40		
5.45	1.49		
6.13	1.58		
6.81	1.65		
7.49	1.72		
8.17	1.78		
8.85	1.83		
9.53	1.88		
10.22	1.91		
10.90	1.94		
11.58	1.96		
12.26	1.98		
12.94	2.00		
13.62	2.00		

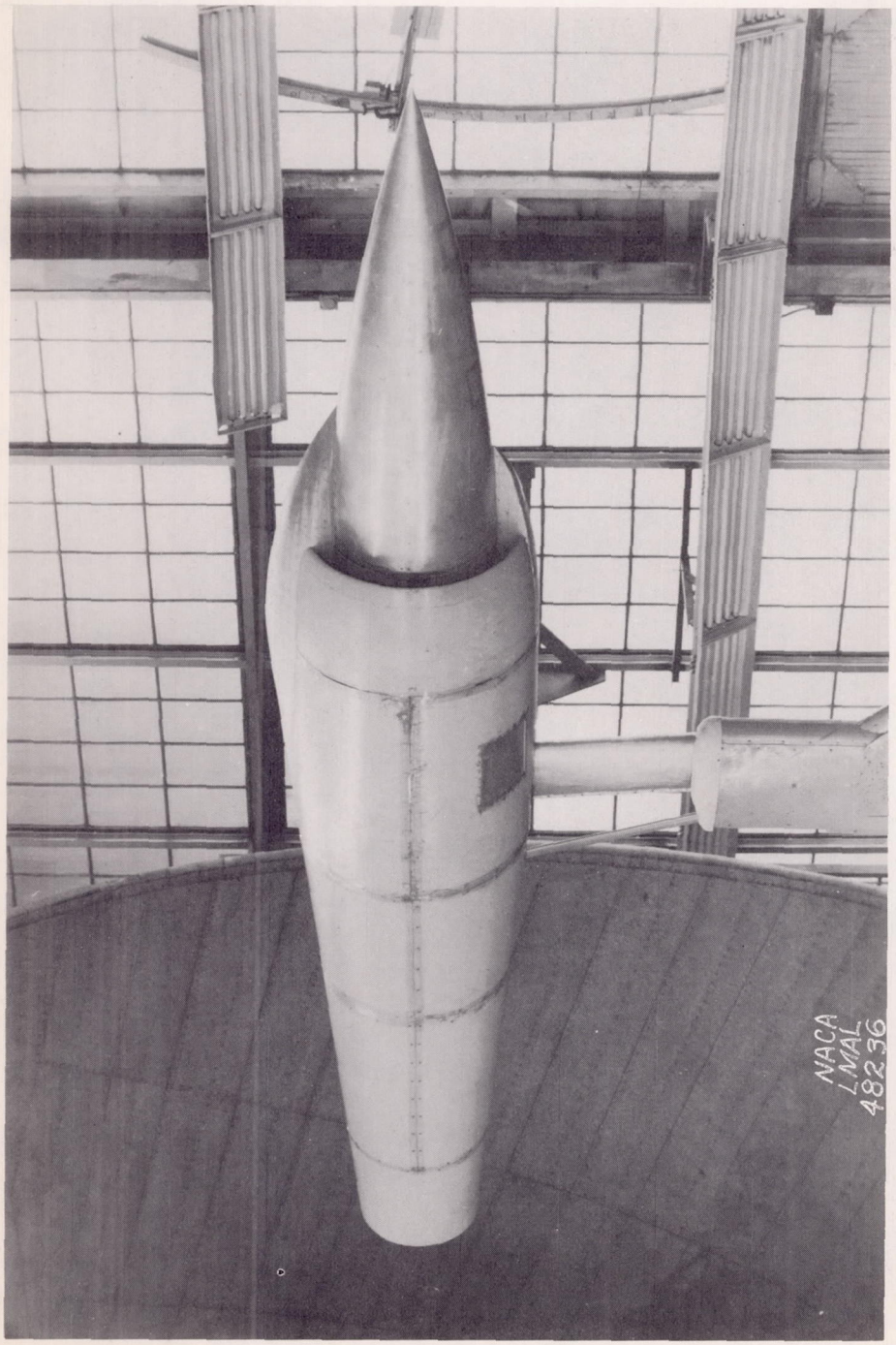

Figure 1.- General view of model mounted in tunnel.

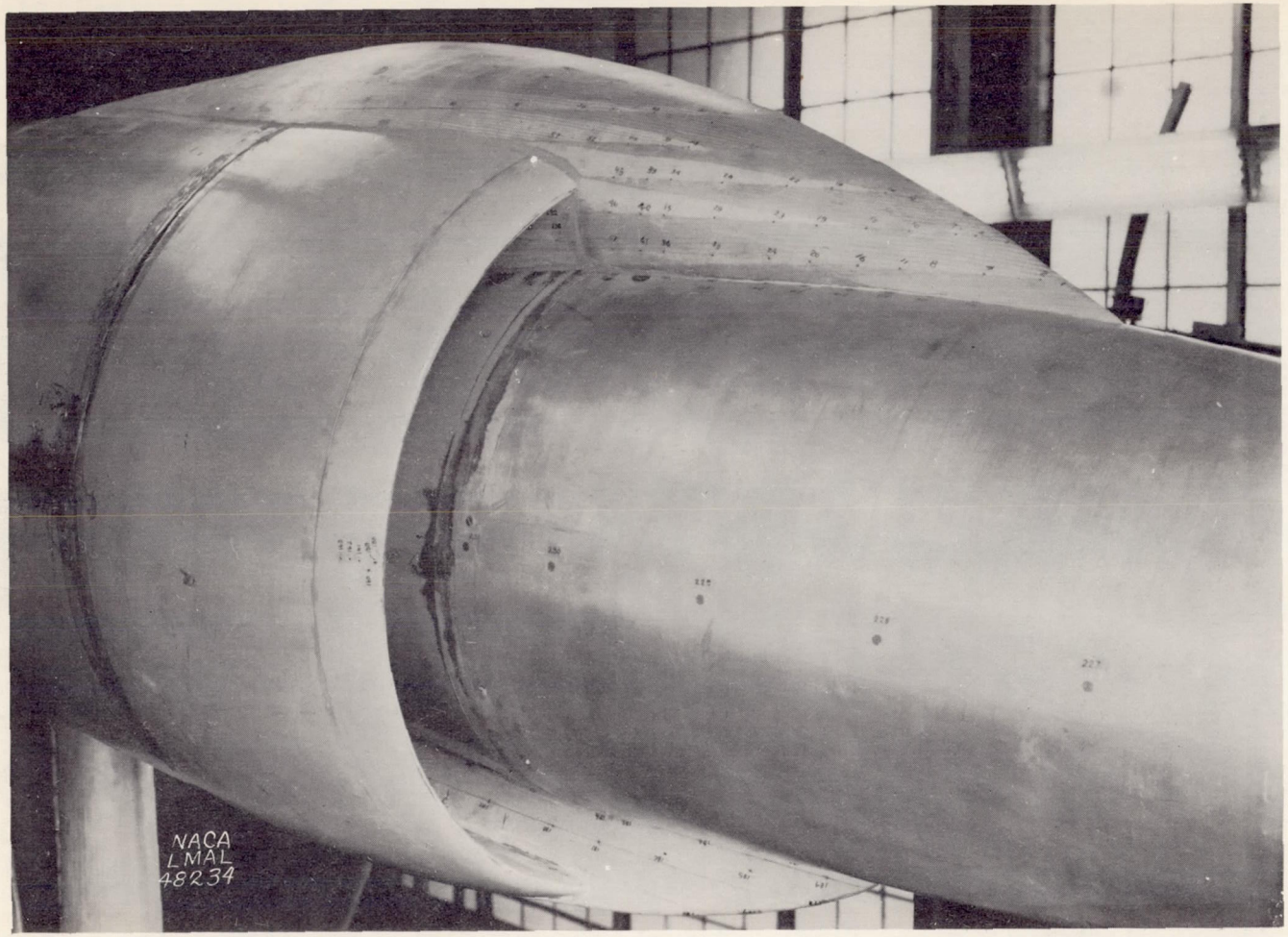

(a) Right side. (Note surface orifices.)

Figure 2.- Detail views of inlet.

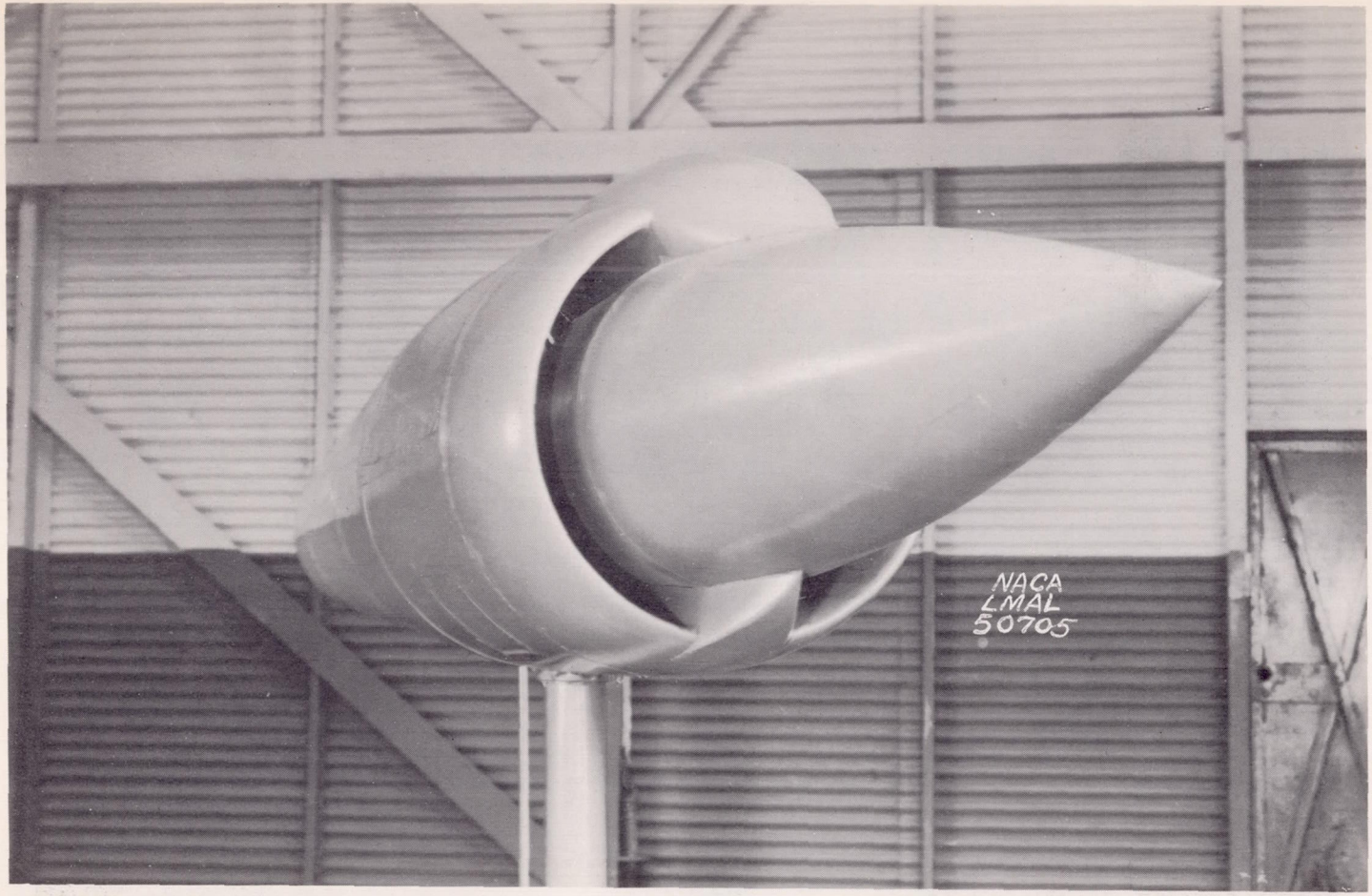

(b) Right side from underneath model.

Figure 2.- Continued.

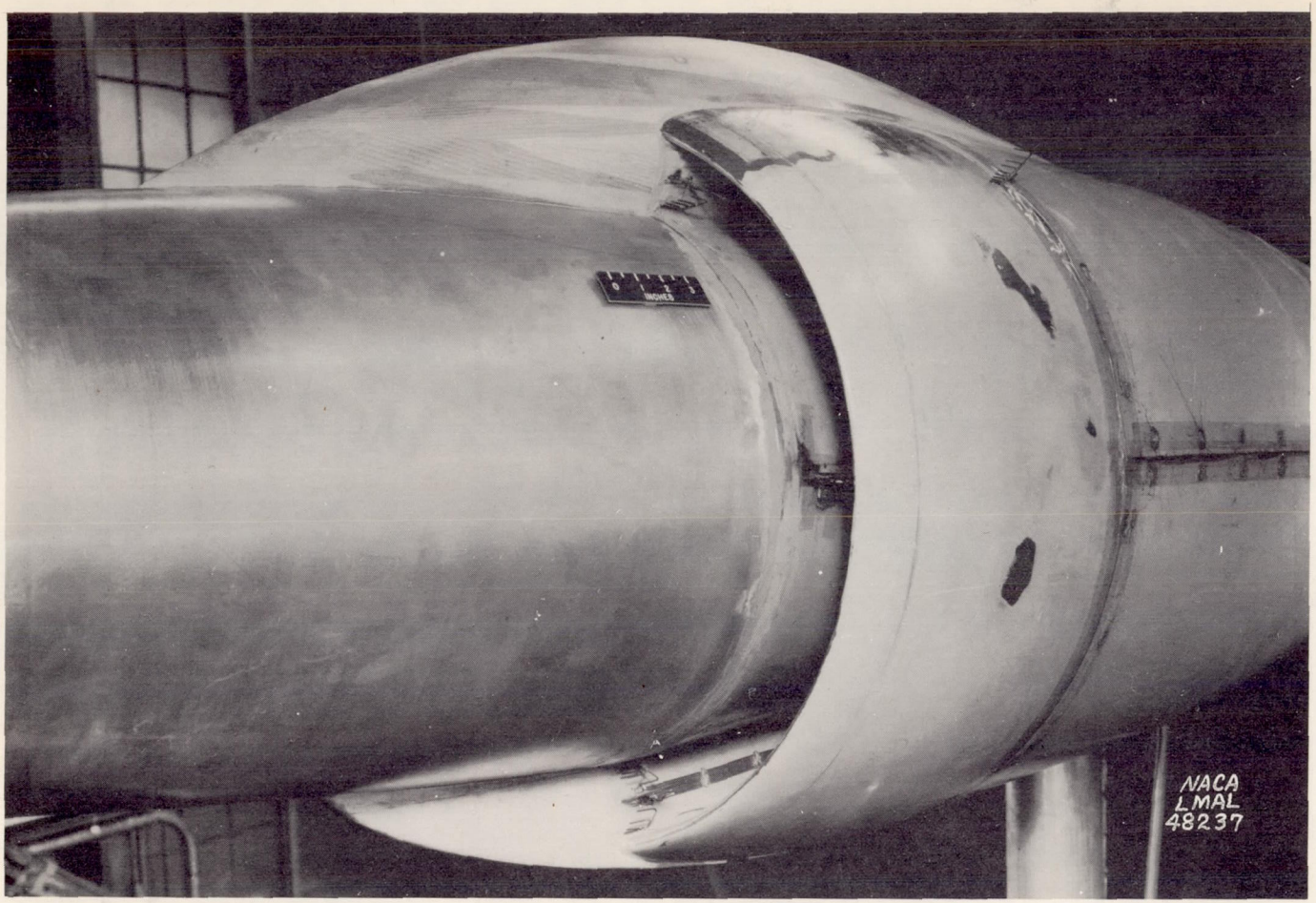

(c) Left side. (Note pressure-survey rakes.)

Figure 2.- Continued.

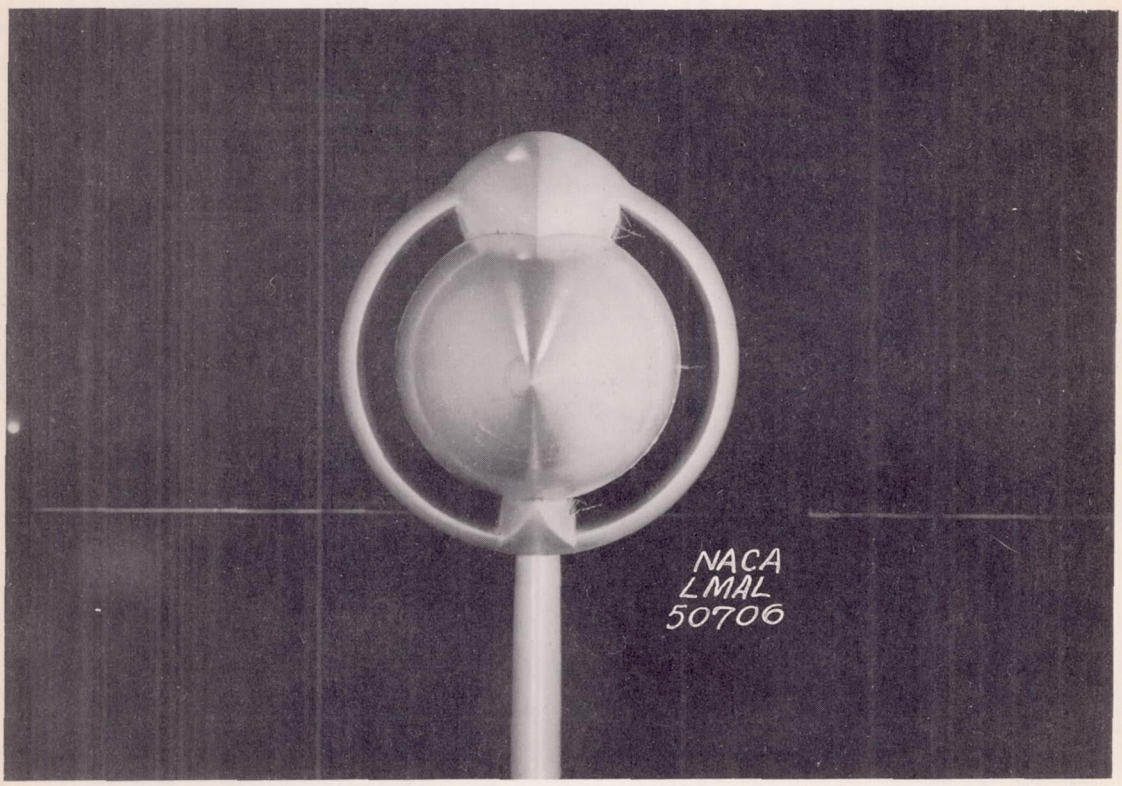

(d) Front.

Figure 2.- Concluded.

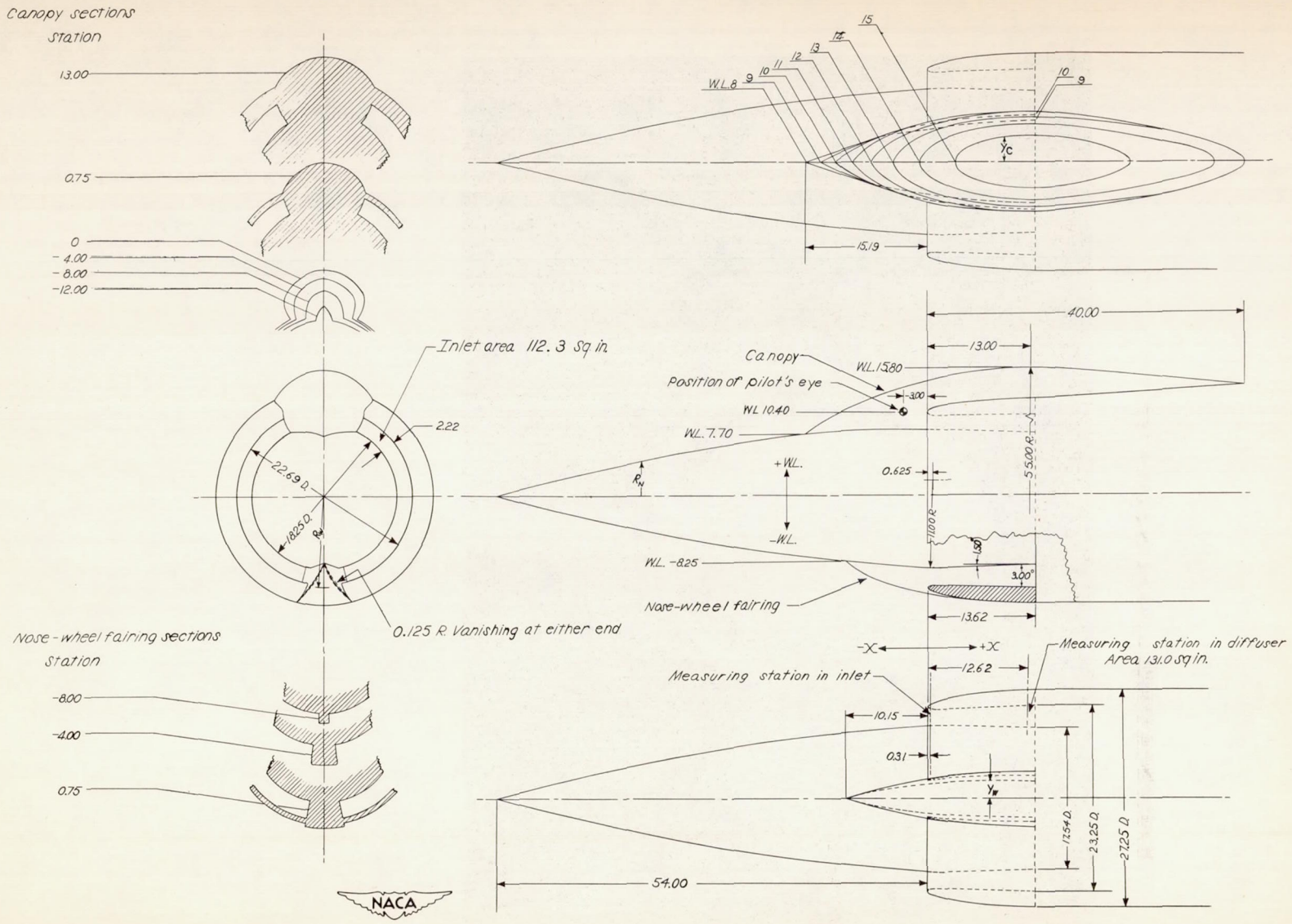

Figure 3.- Arrangement and dimensions of nose section of model.
All dimensions are in inches.

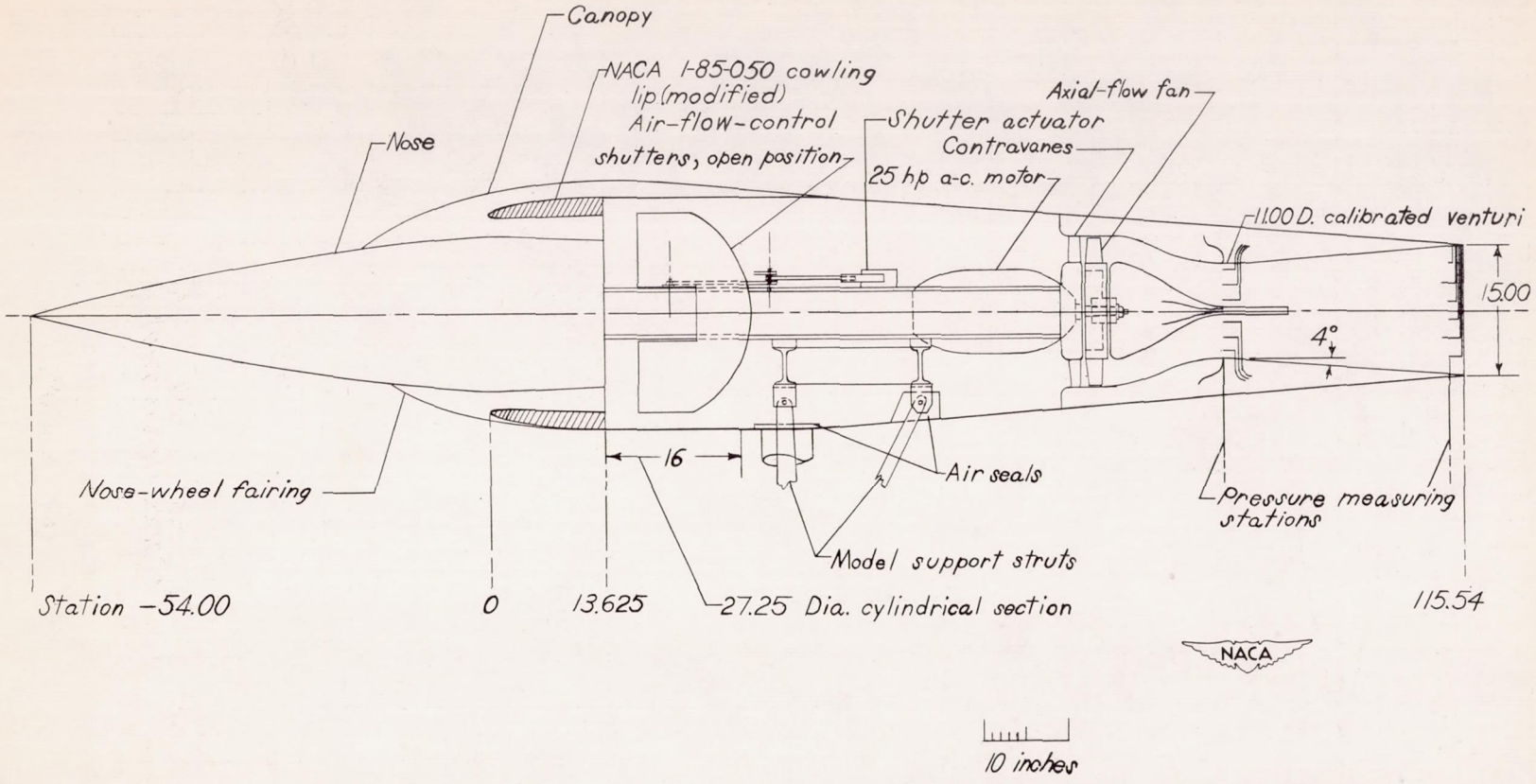

Figure 4.- Schematic drawing of model showing internal arrangement.
All dimensions are in inches.

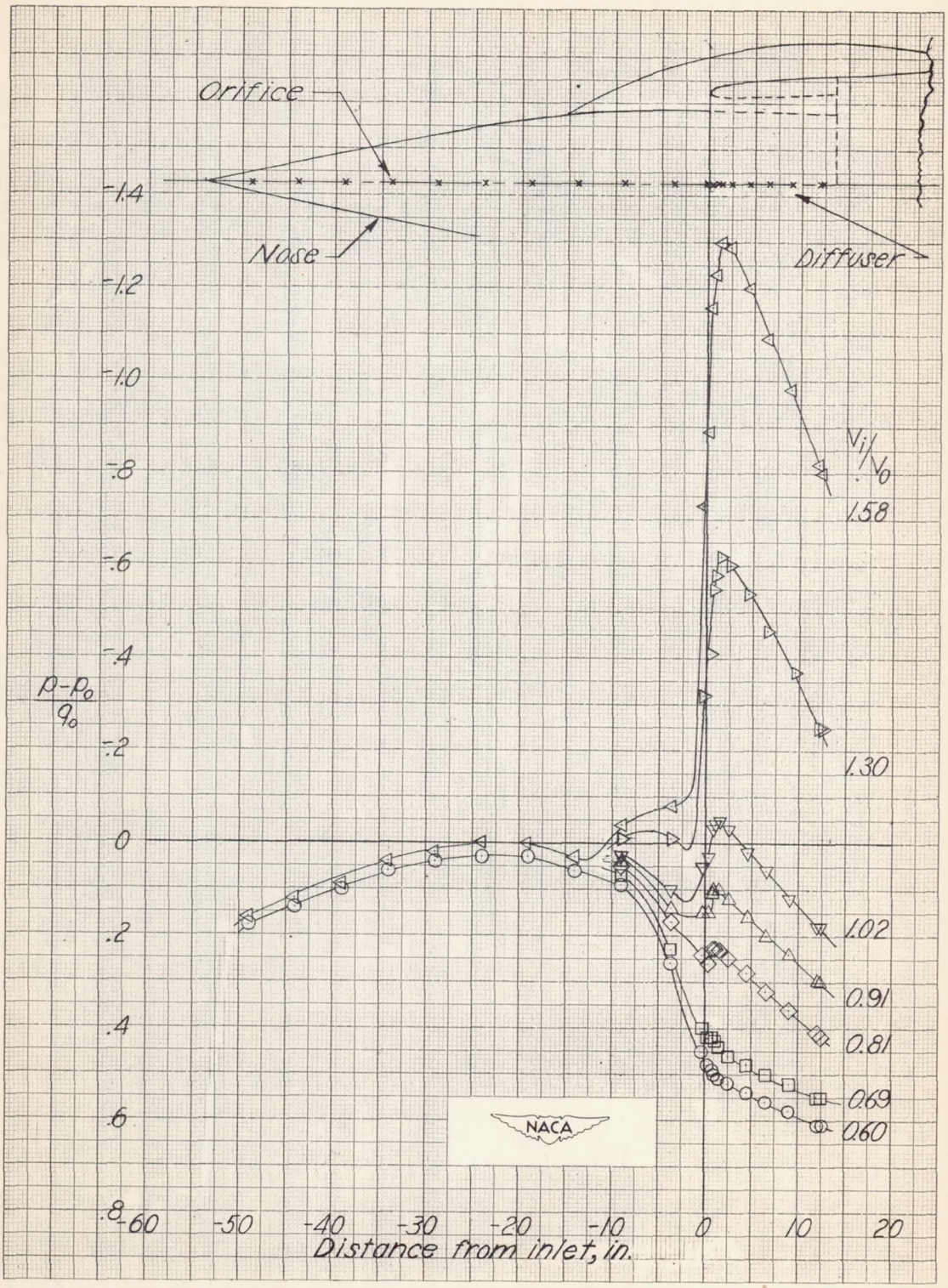

(a) $\alpha = 0^{\circ}$.

Figure 5.- Static-pressure distributions over nose and inner surface of diffuser at horizontal center line of model.

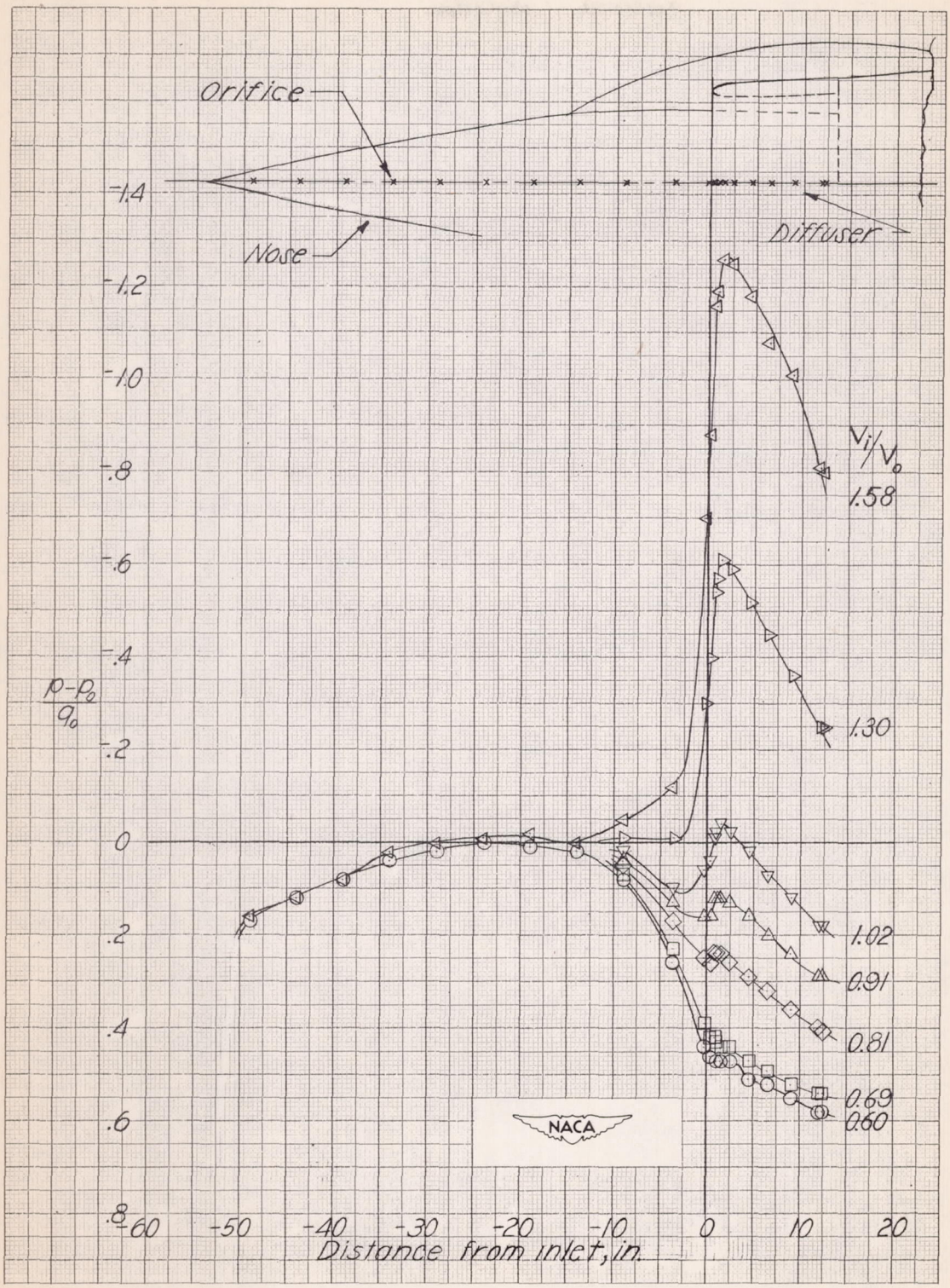

(b) $\alpha = 3^{\circ}$.

Figure 5.- Continued.

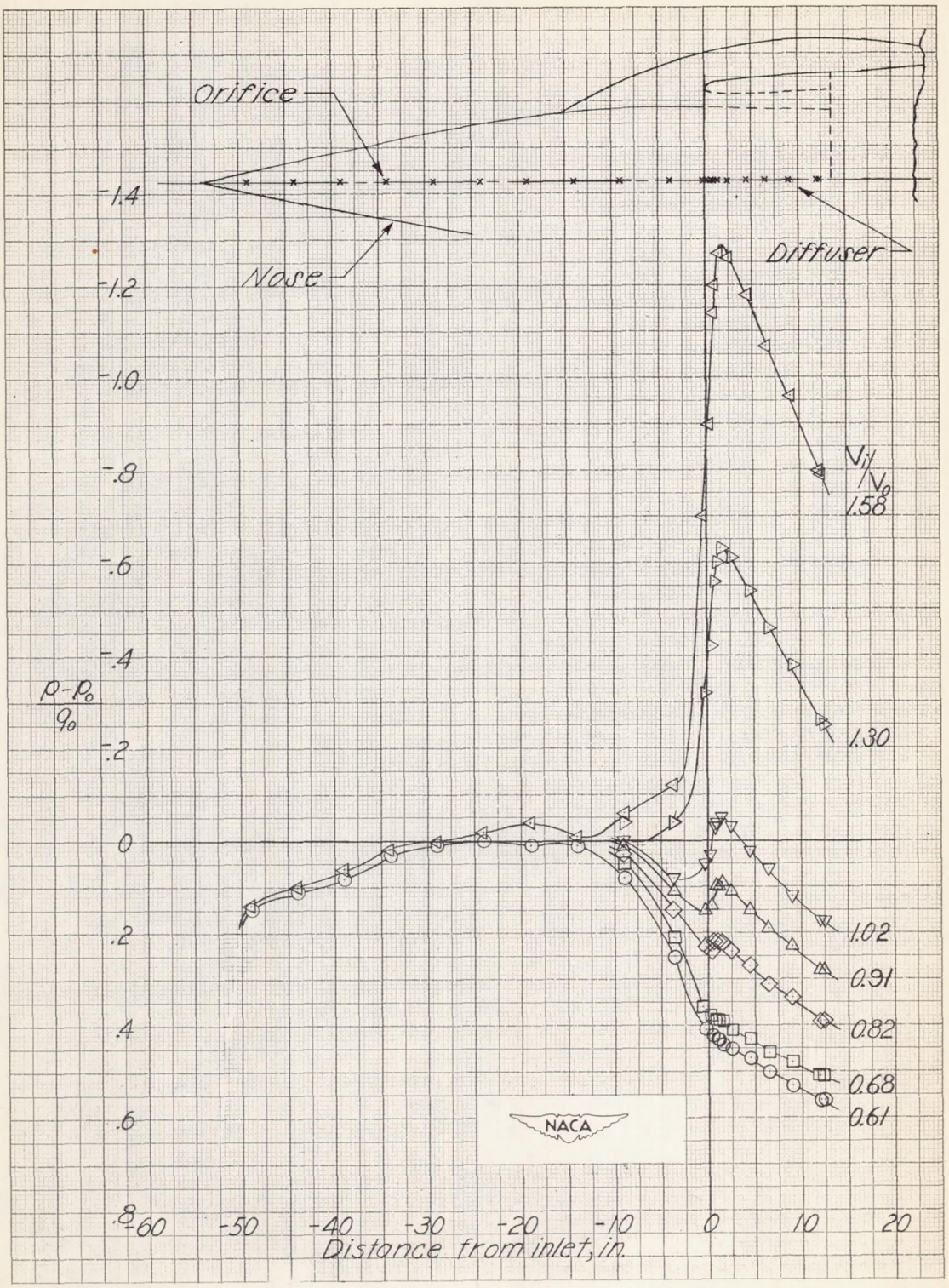

(c) $\alpha = 6^{\circ}$.

Figure 5.- Concluded.

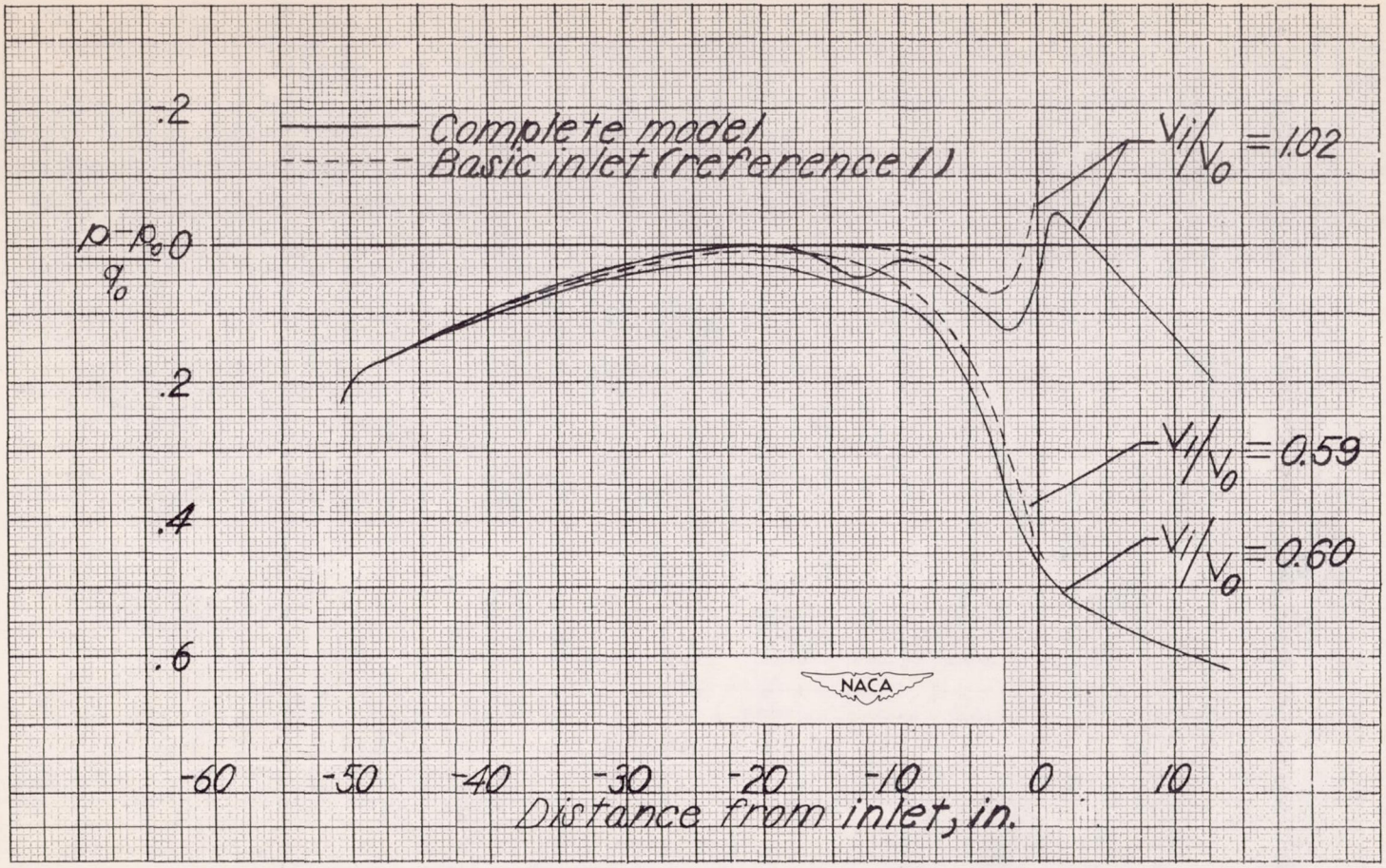

Figure 6.- Comparison of static-pressure distributions on side of nose with corresponding static-pressure distributions measured on top of nose of basic inlet in reference 1. $\alpha = 0^{\circ}$.

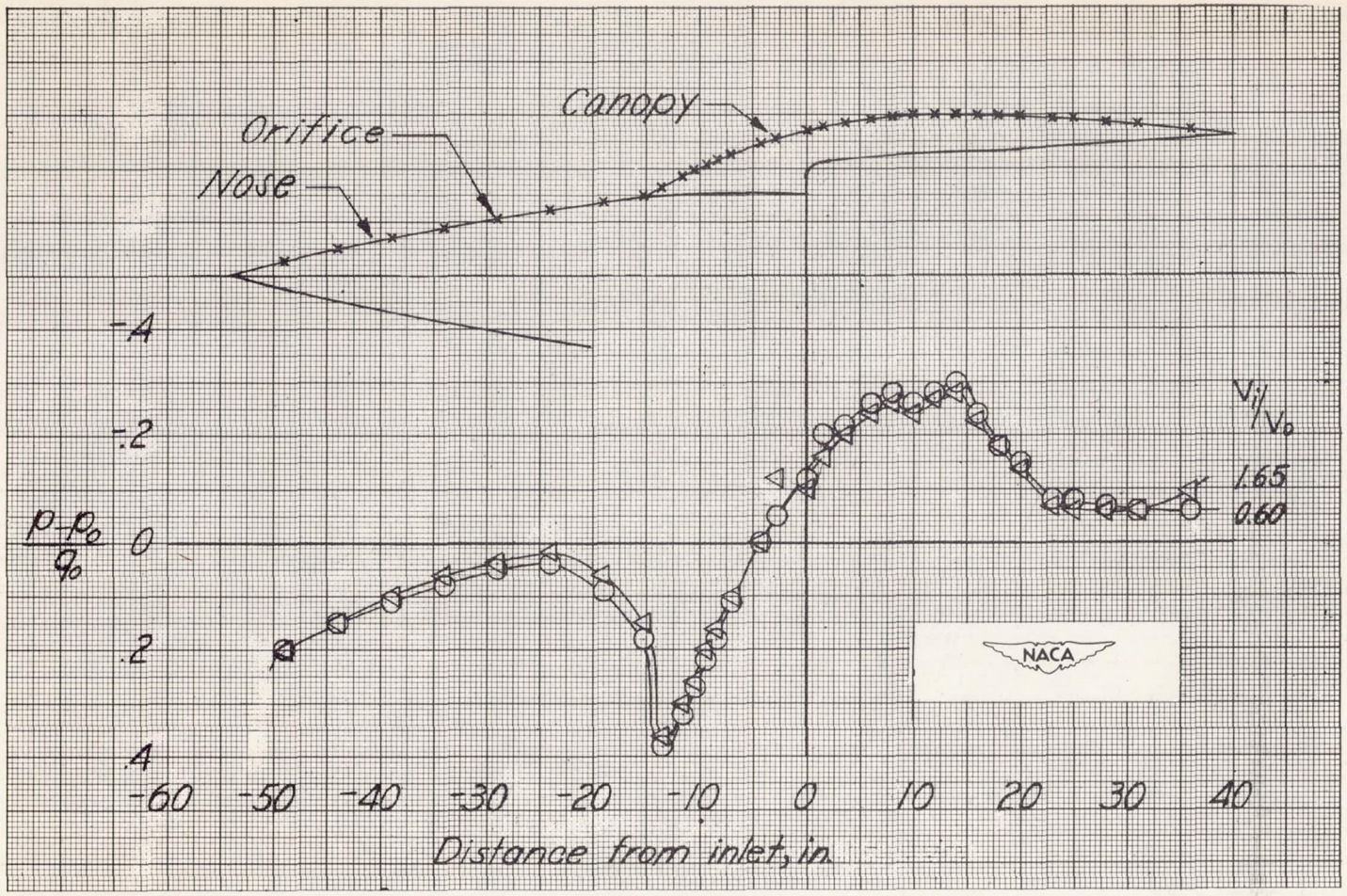

(a) $\alpha = 0^\circ$.

Figure 7.- Static-pressure distributions over top of nose and canopy.

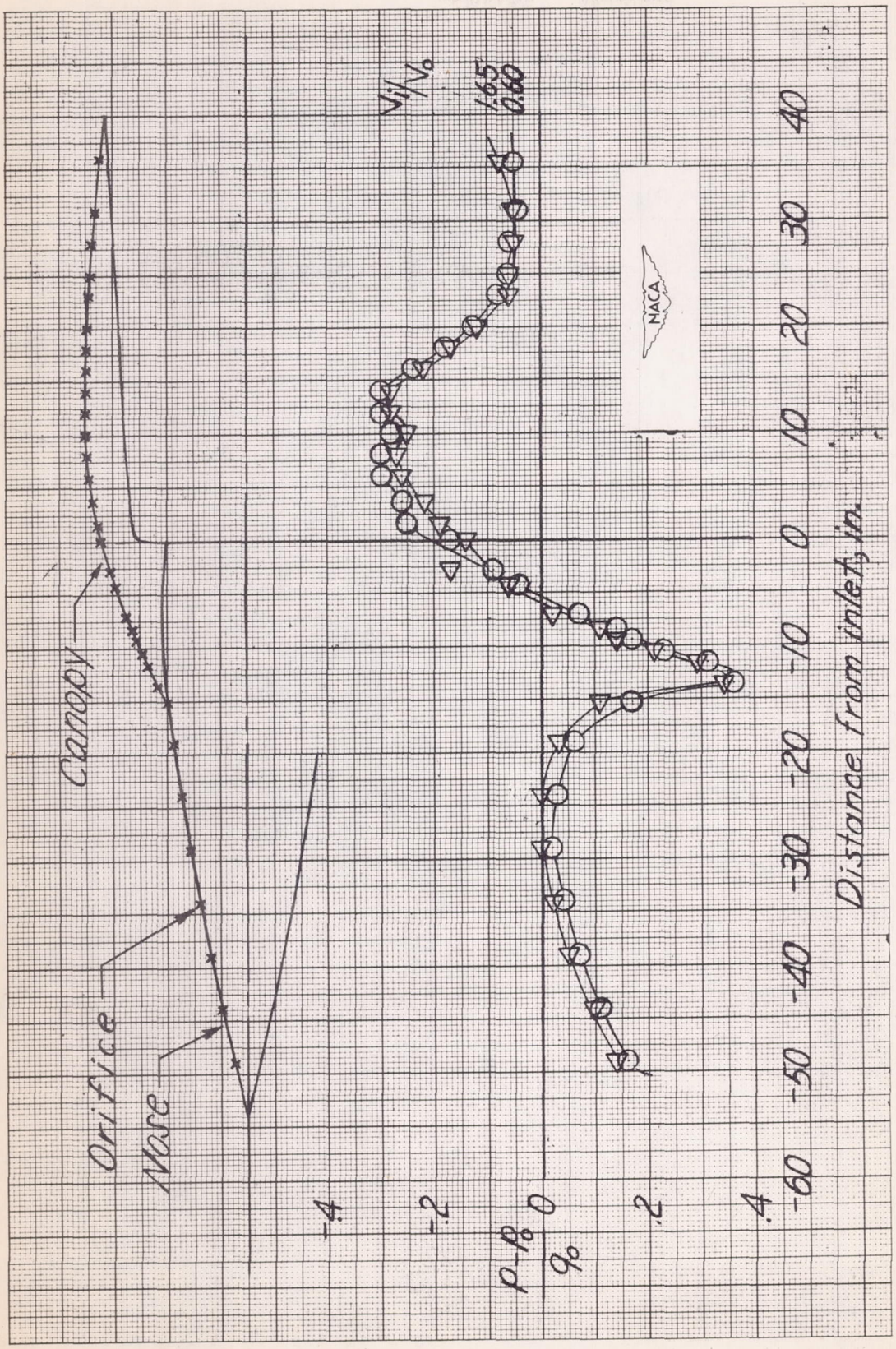

(b) $\alpha = 3^{\circ}$.

Figure 7.- Continued.

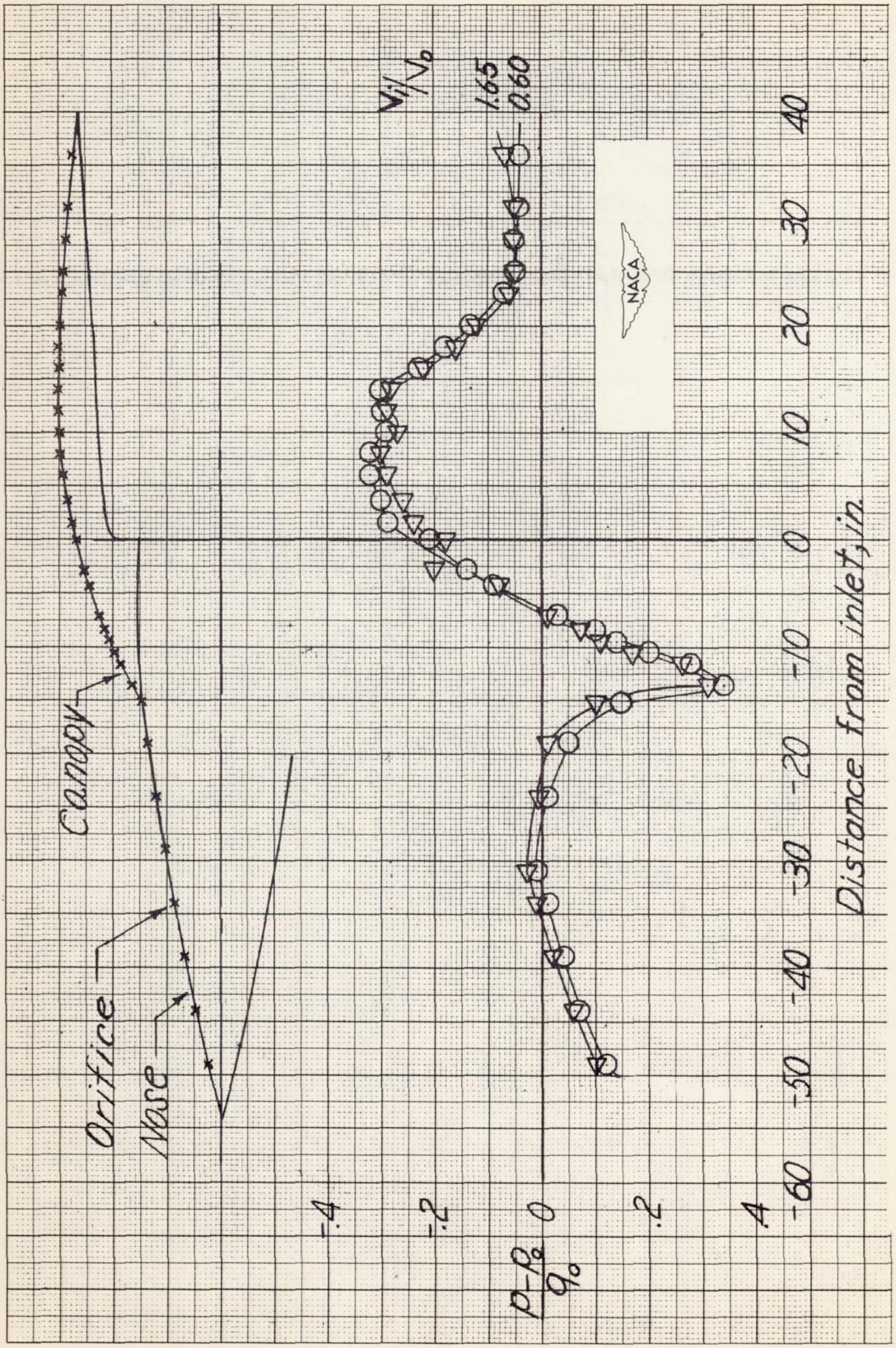

(c) $\alpha = 6^\circ$.

Figure 7.- Concluded.

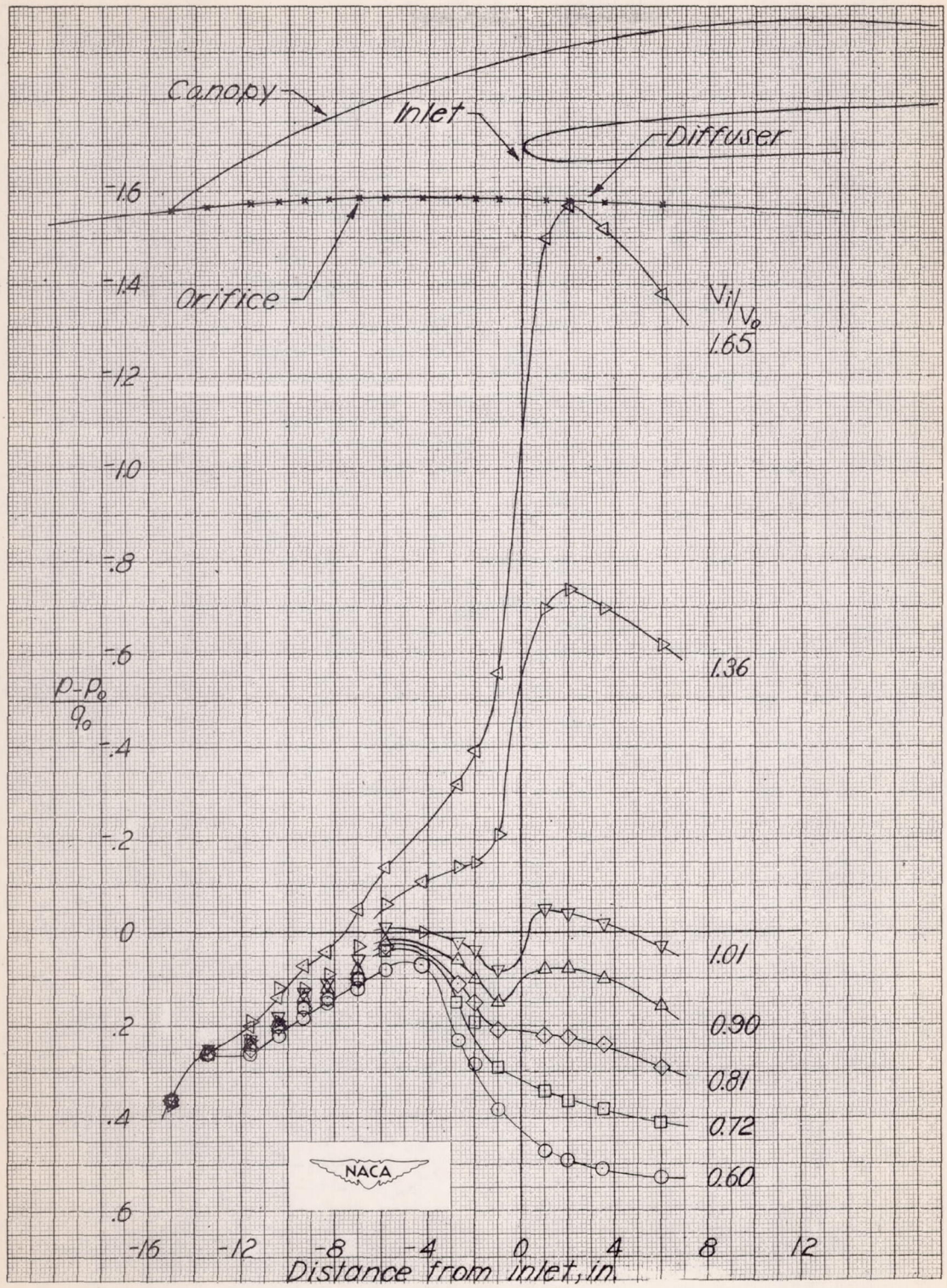

(a) $\alpha = 0^\circ$.

Figure 8.- Static-pressure distributions at intersection of canopy with nose and inner surface of diffuser.

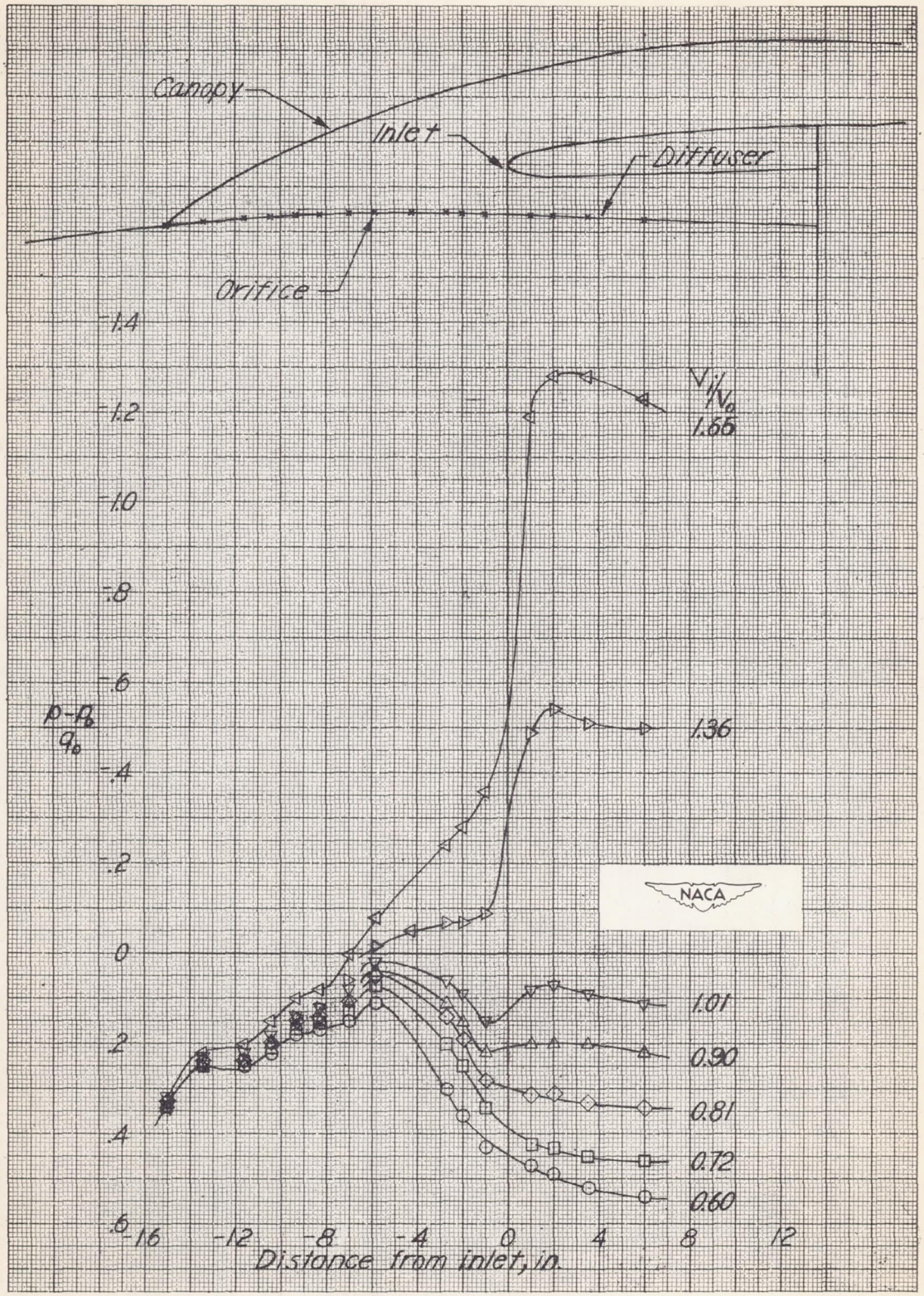

(b) $\alpha = 3^{\circ}$.

Figure 8.- Continued.

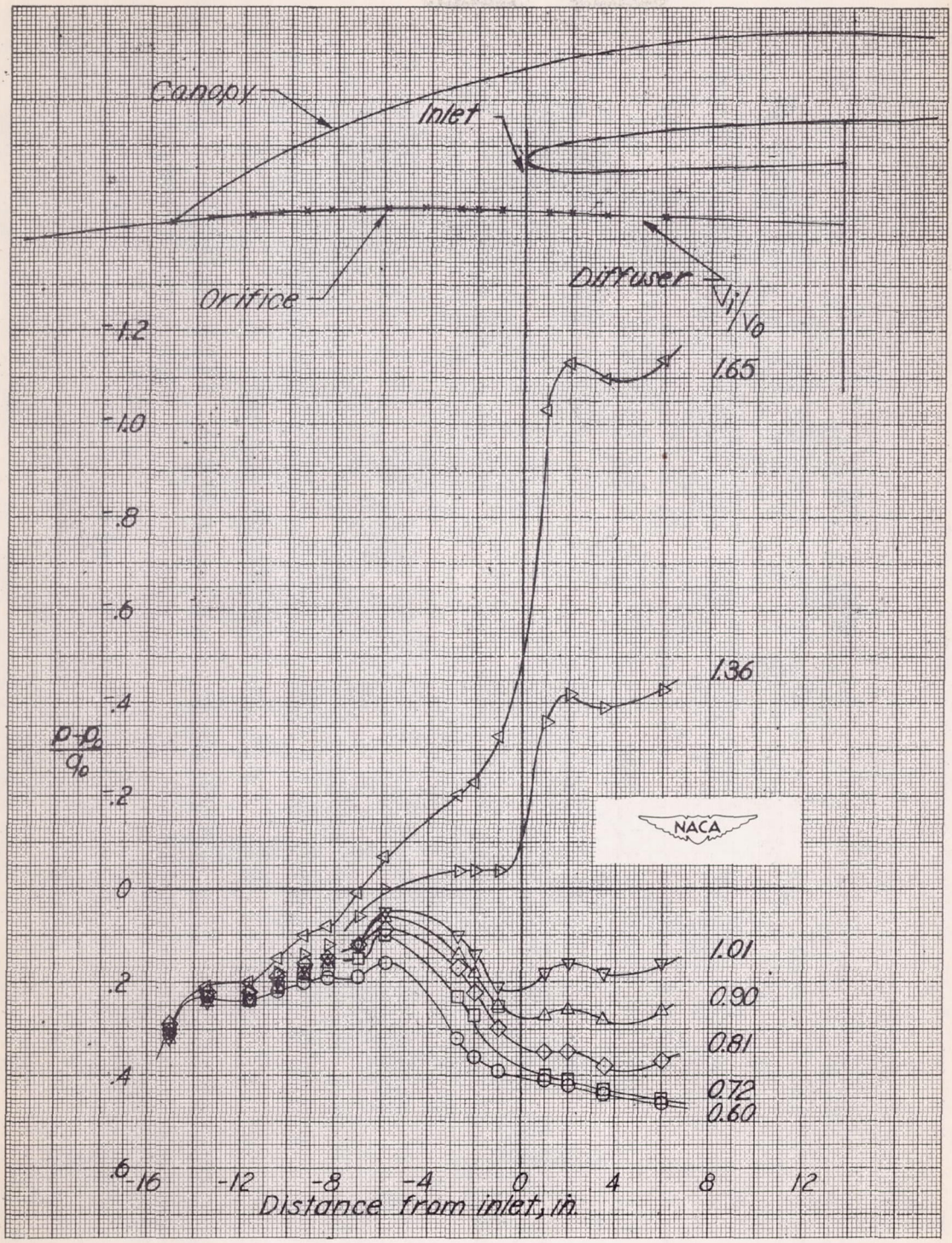

(c) $\alpha = 6^{\circ}$.

Figure 8.- Concluded.

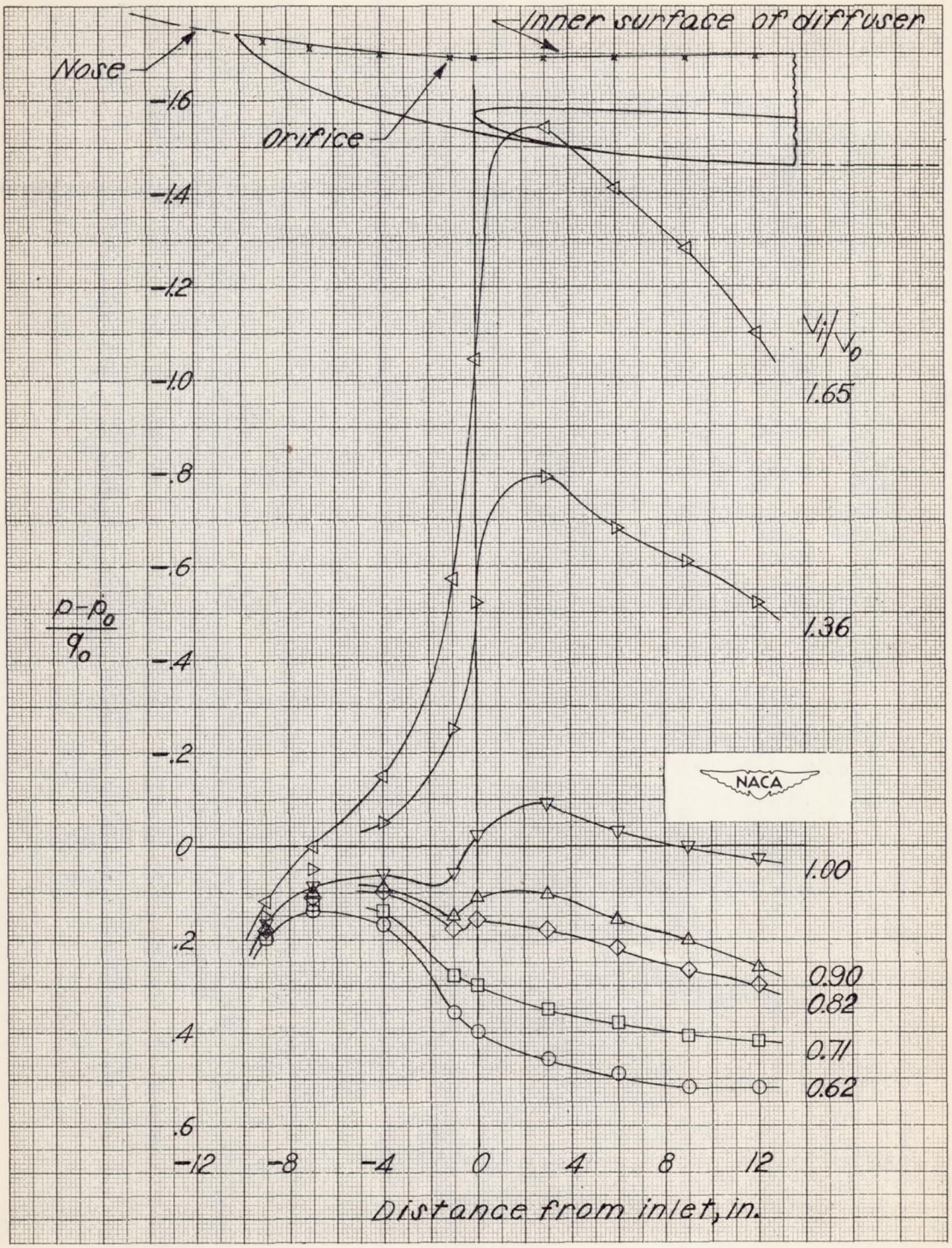

(a) $\alpha = 0^{\circ}$.

Figure 9.- Static-pressure distributions at intersection of nose-wheel fairing with nose and inner surface of diffuser.

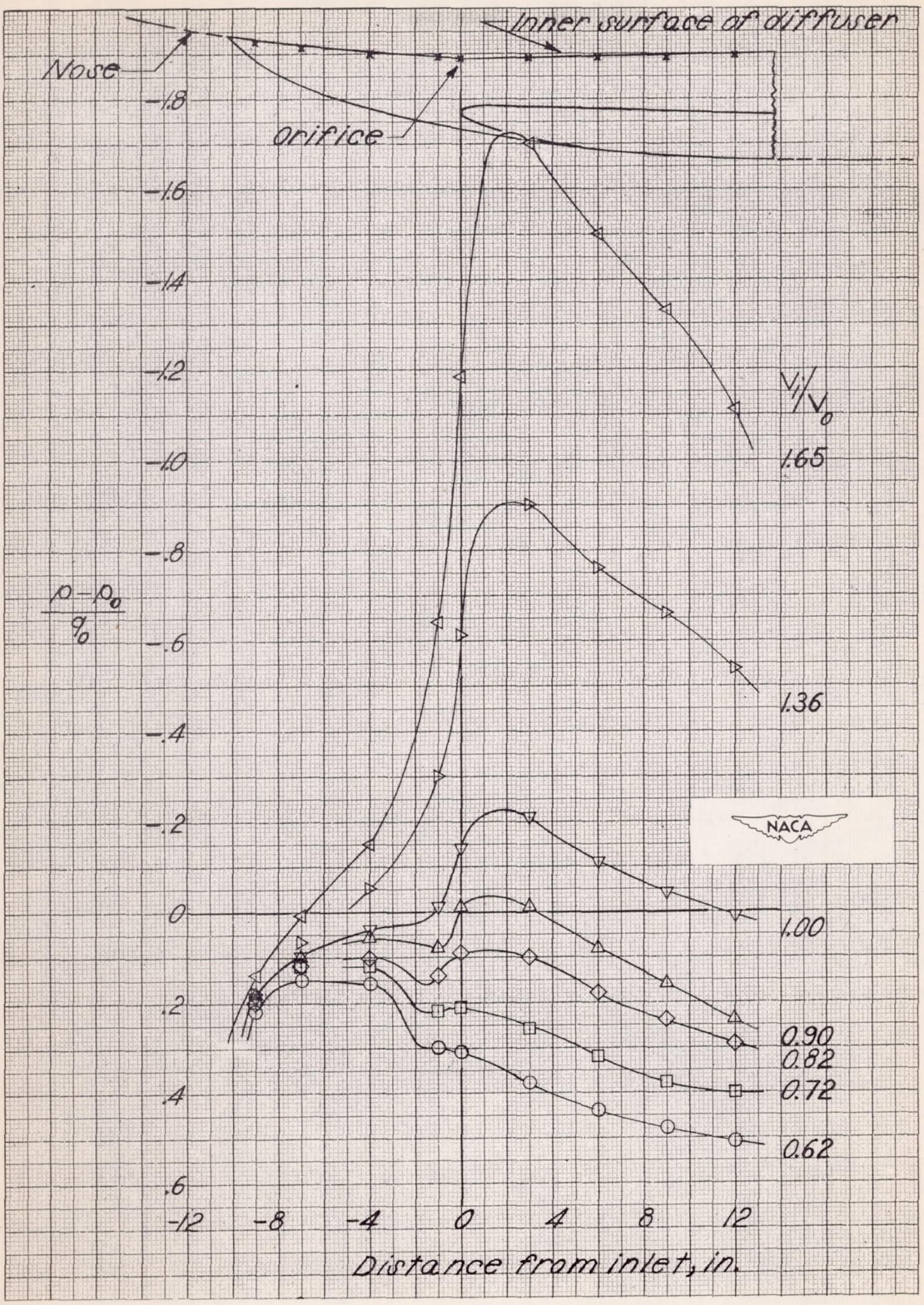

(b) $\alpha = 3^{\circ}$.

Figure 9.- Continued.

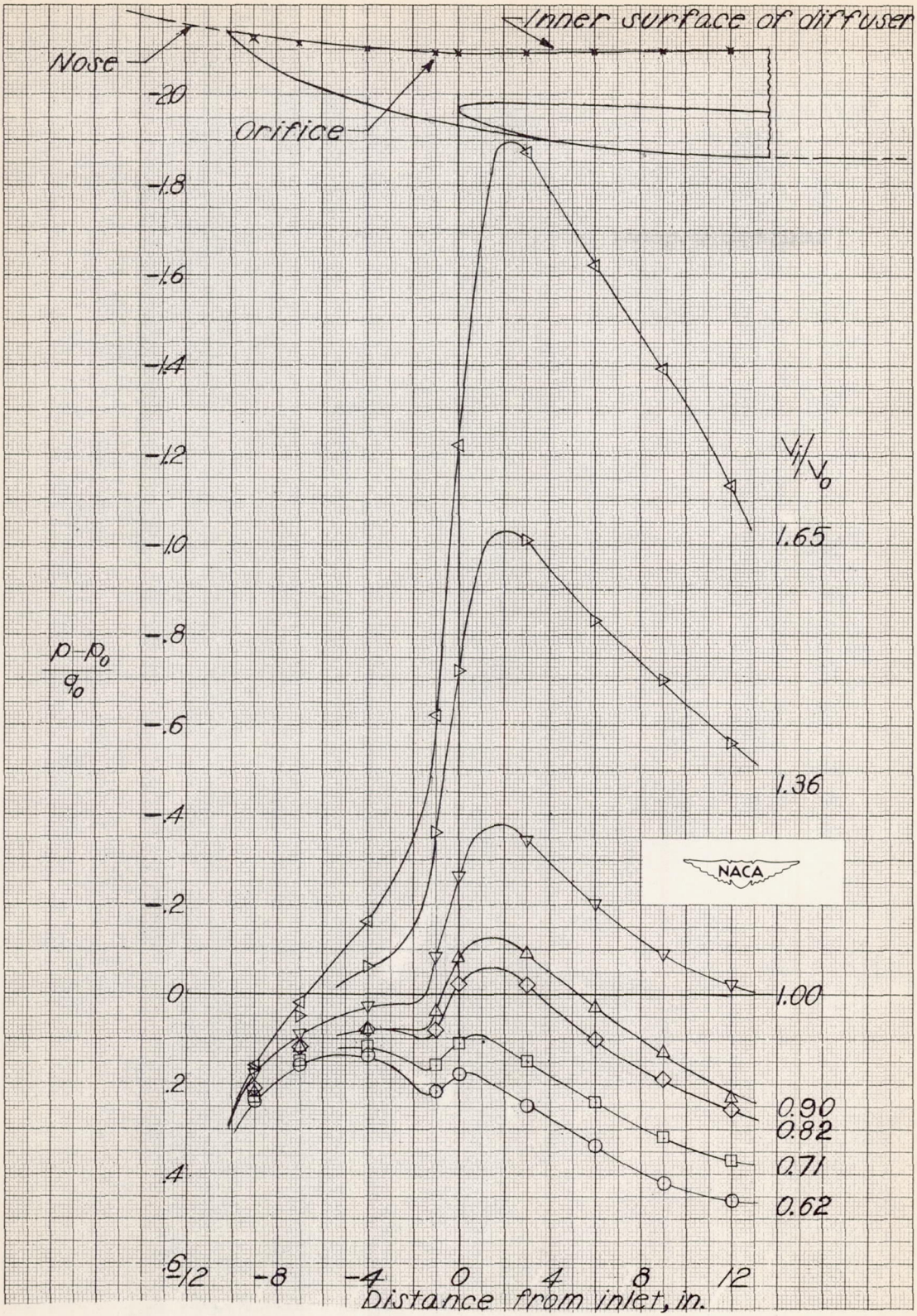

(c) $\alpha = 6^\circ$.

Figure 9.- Concluded.

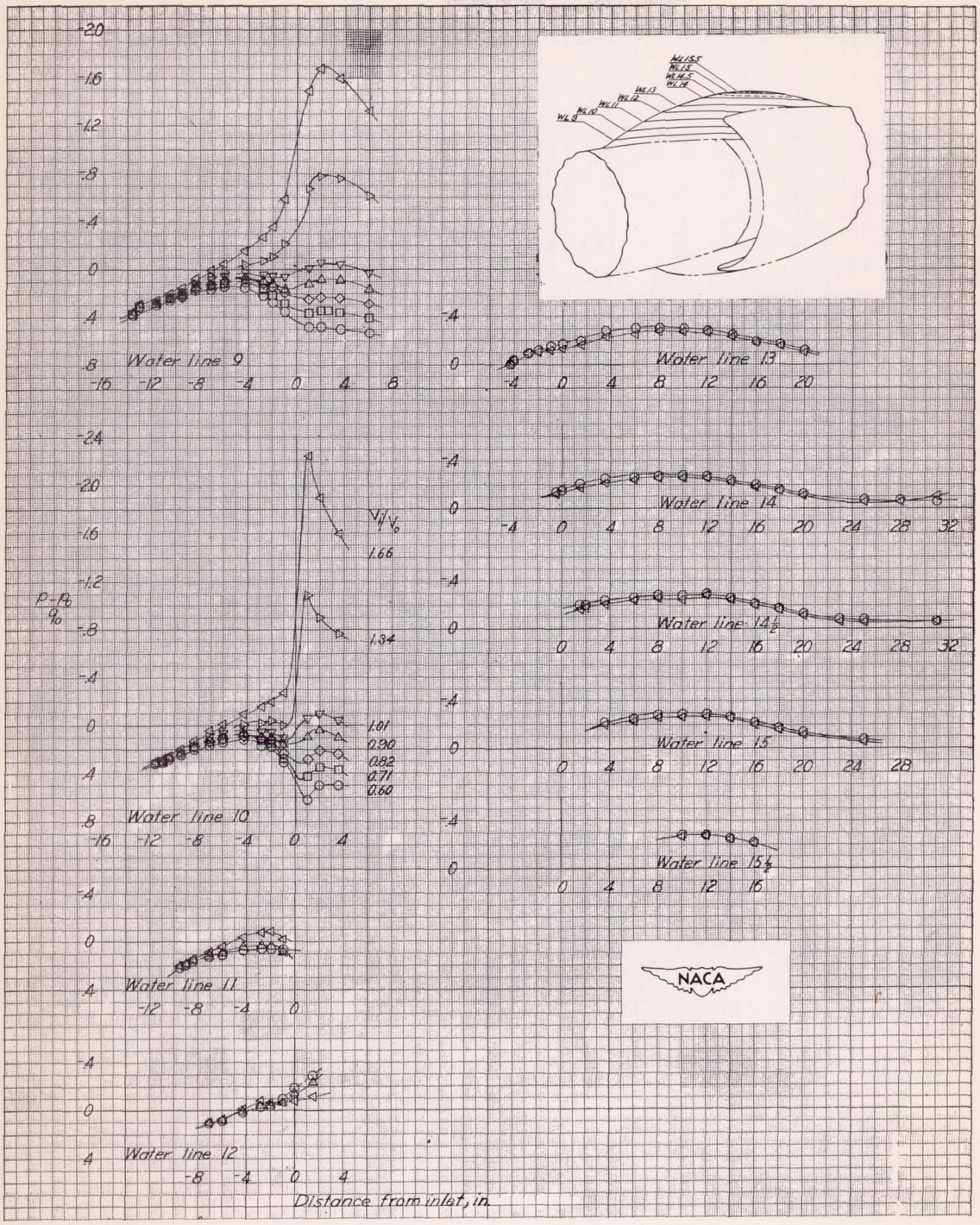

(a) $\alpha = 0^{\circ}$.

Figure 10.- Static-pressure distribution on canopy contours.

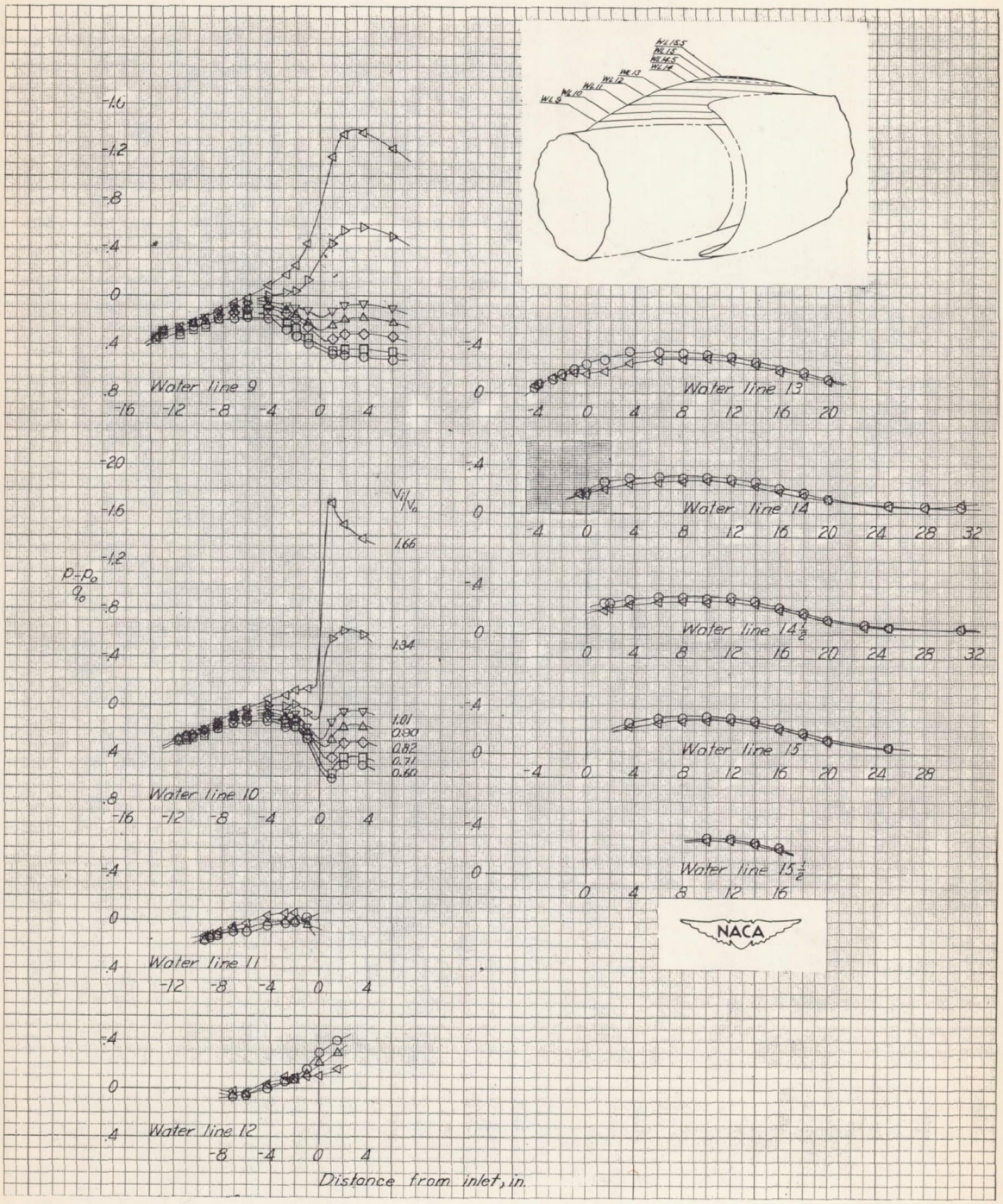

(b) $\alpha = 3^{\circ}$.

Figure 10.- Continued.

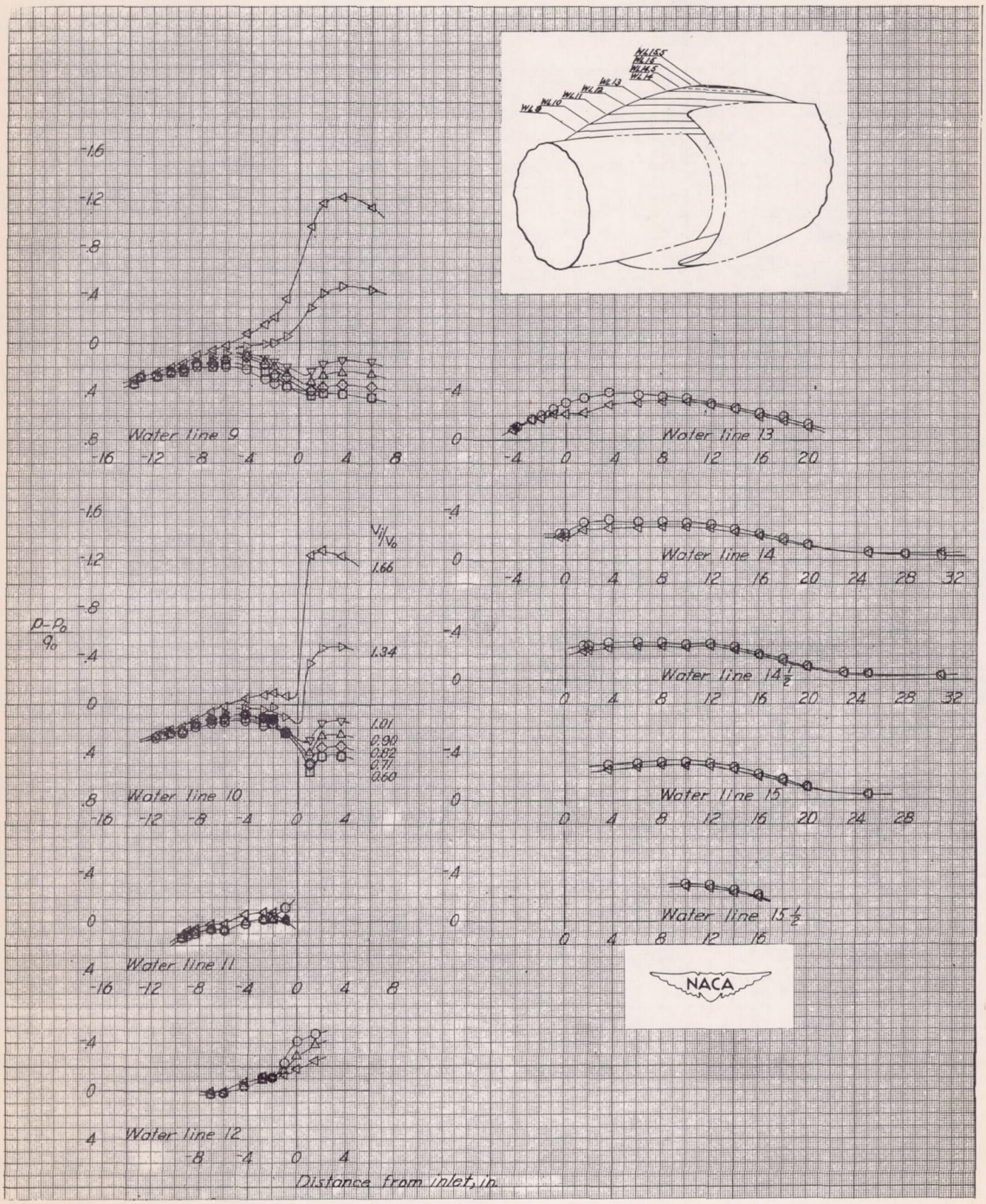

(c) $\alpha = 6^{\circ}$.

Figure 10.- Concluded.

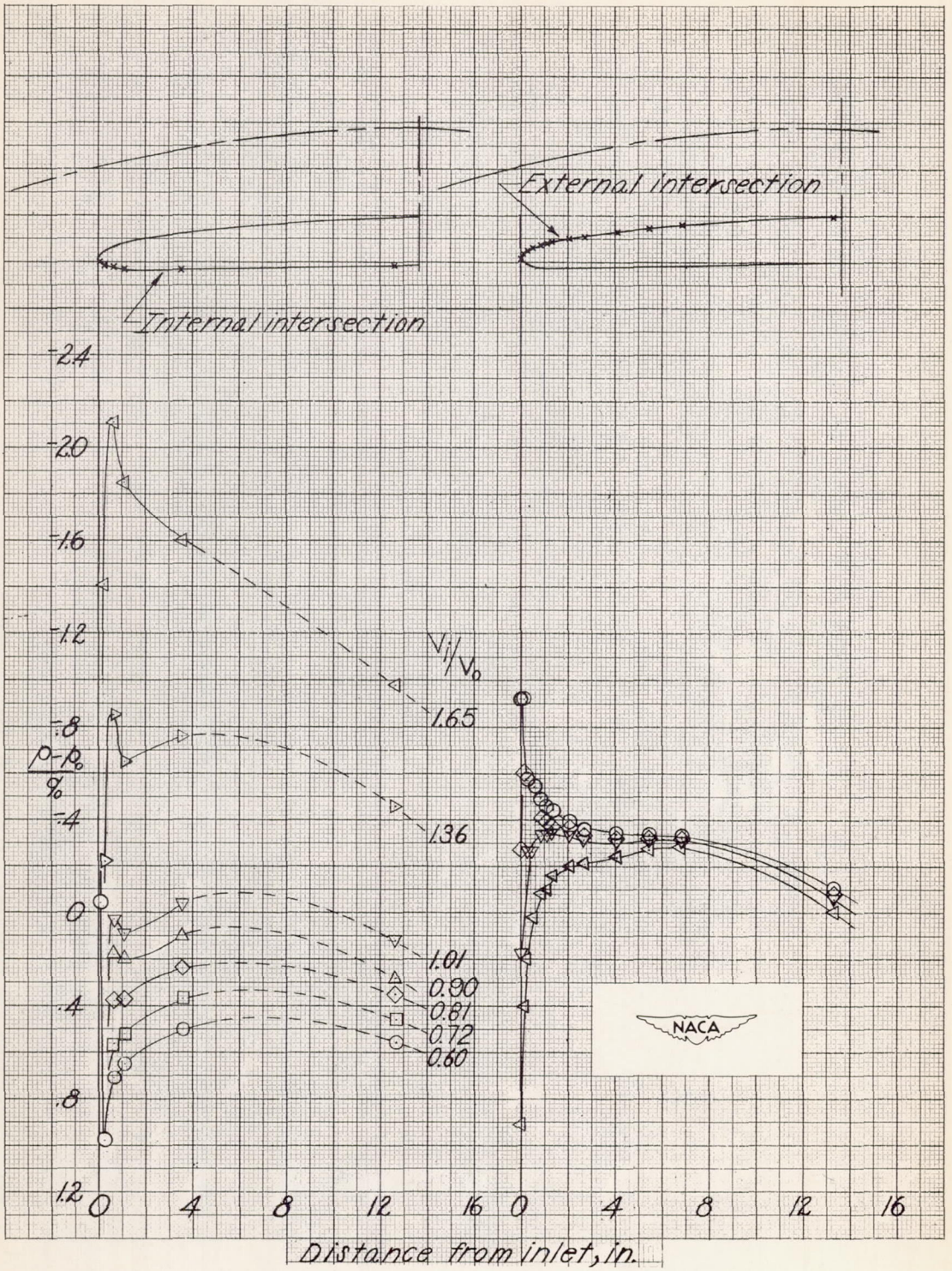

(a) $\alpha = 0^\circ$.

Figure 11.- Static-pressure distributions at intersection of canopy with inlet lip.

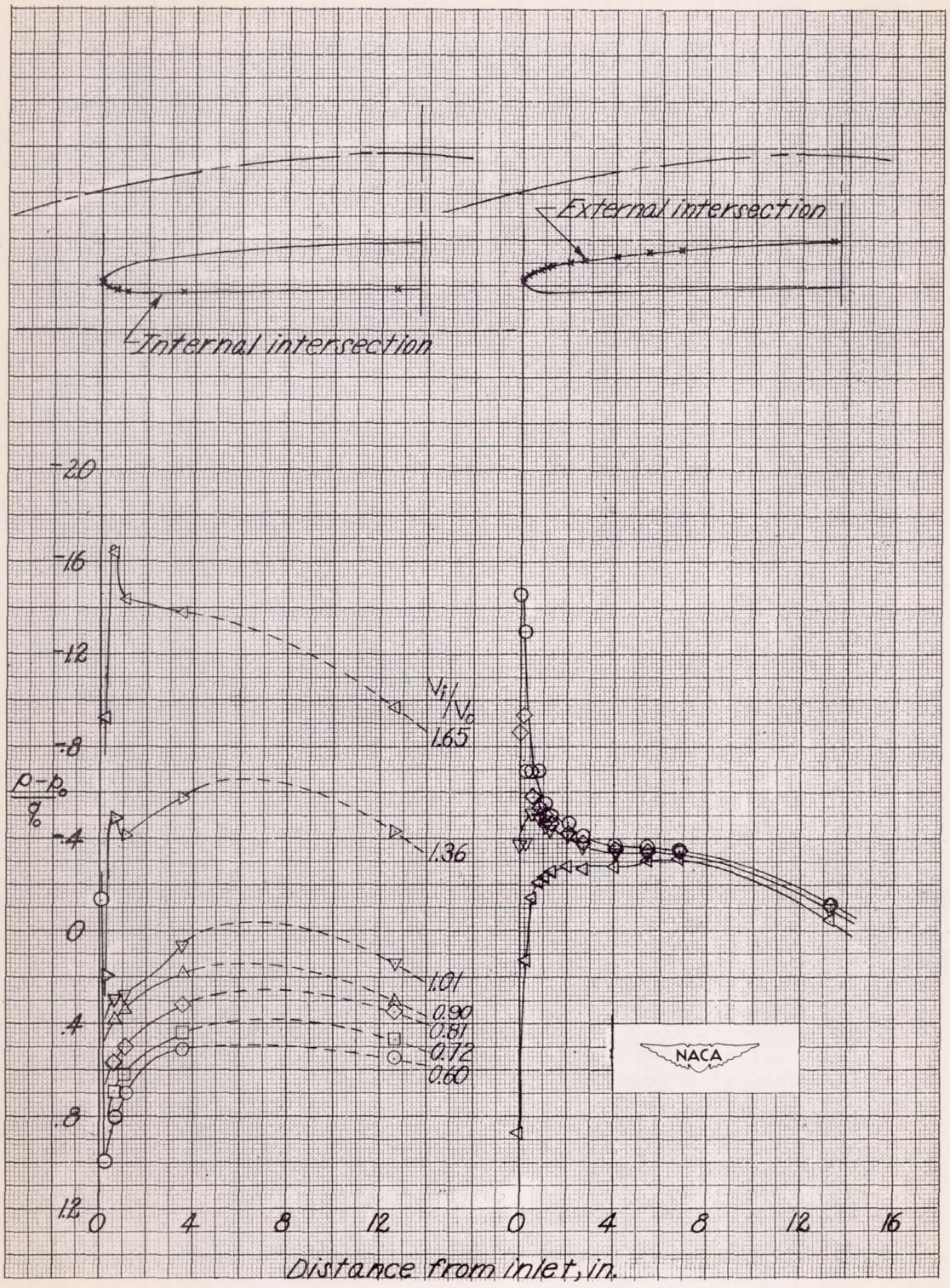

(b) $\alpha = 3^{\circ}$.

Figure 11.- Continued.

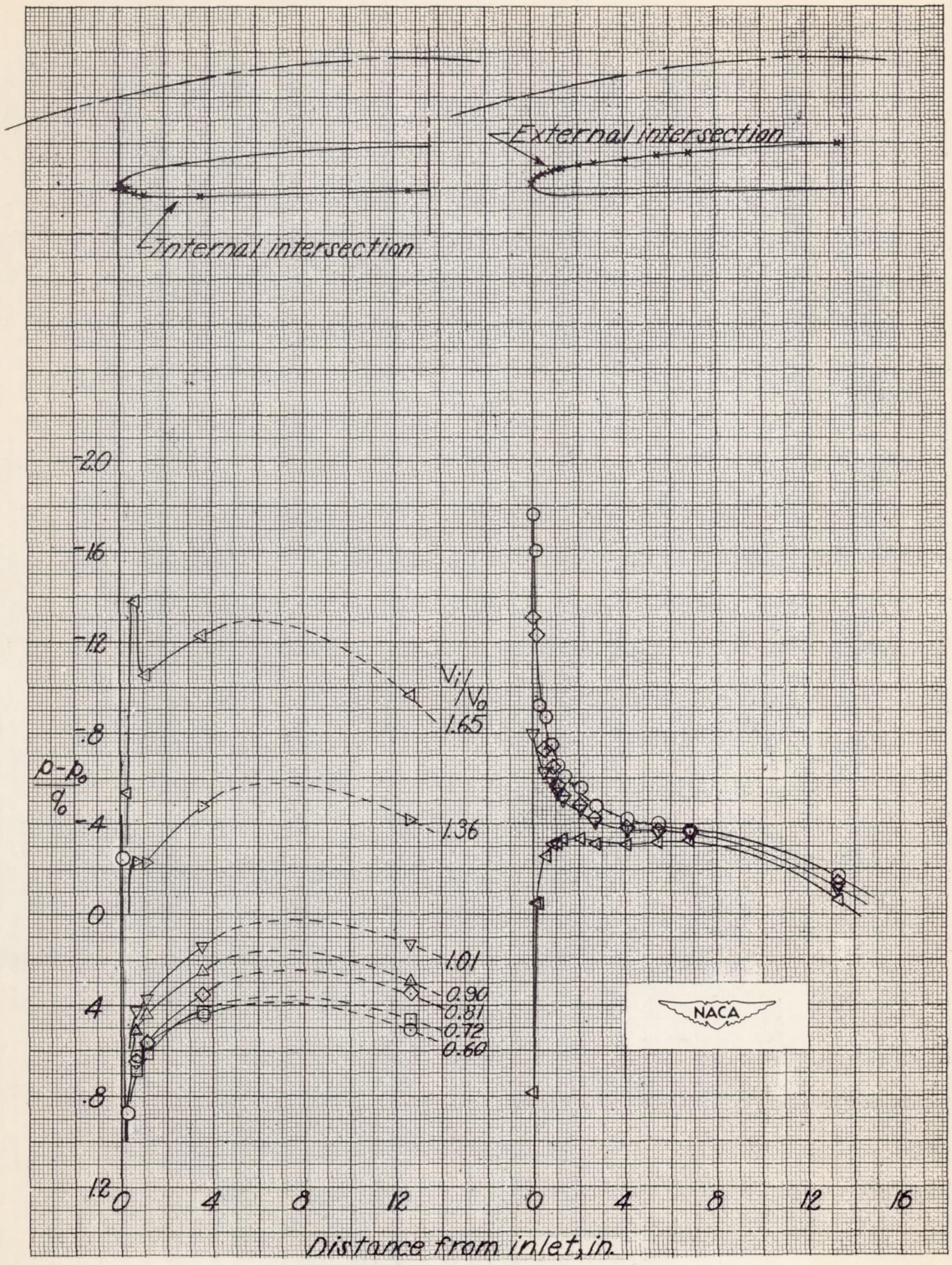

(c) $\alpha = 6^{\circ}$.

Figure 11.- Concluded.

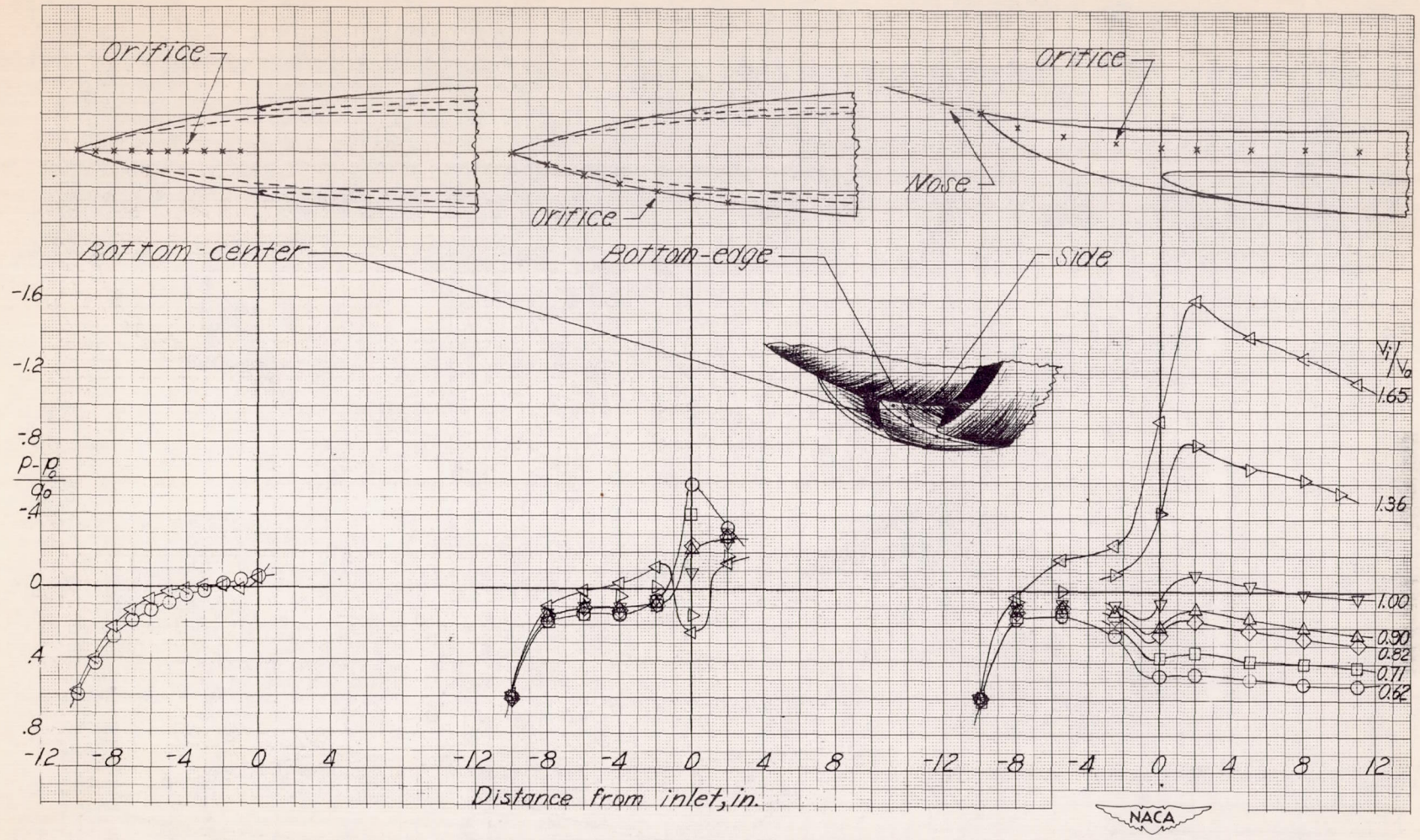

(a) $\alpha = 0^{\circ}$.

Figure 12.- Static-pressure distributions on nose-wheel fairing.

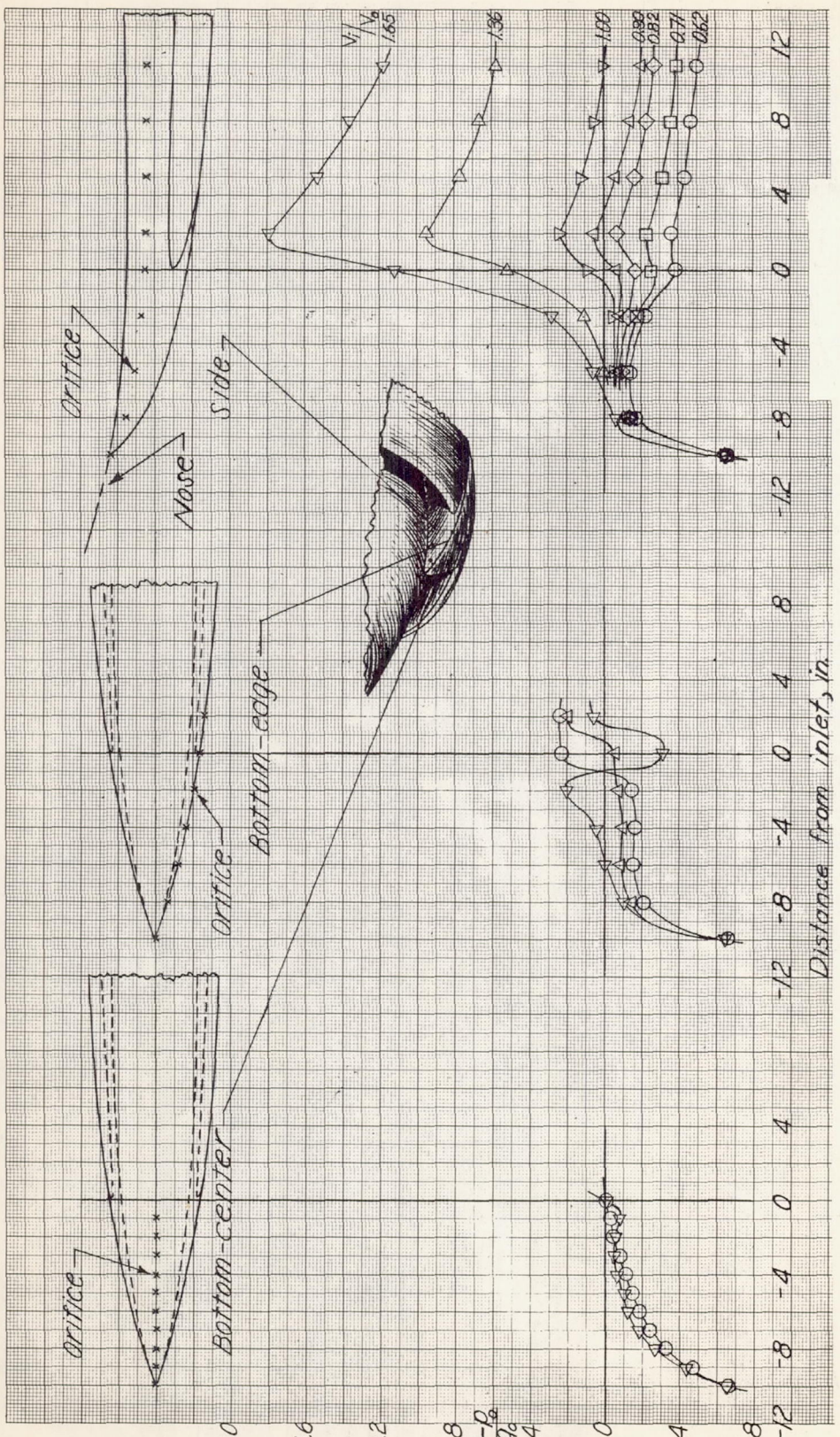

(b) $\alpha = 3^{\circ}$.

Figure 12.- Continued.

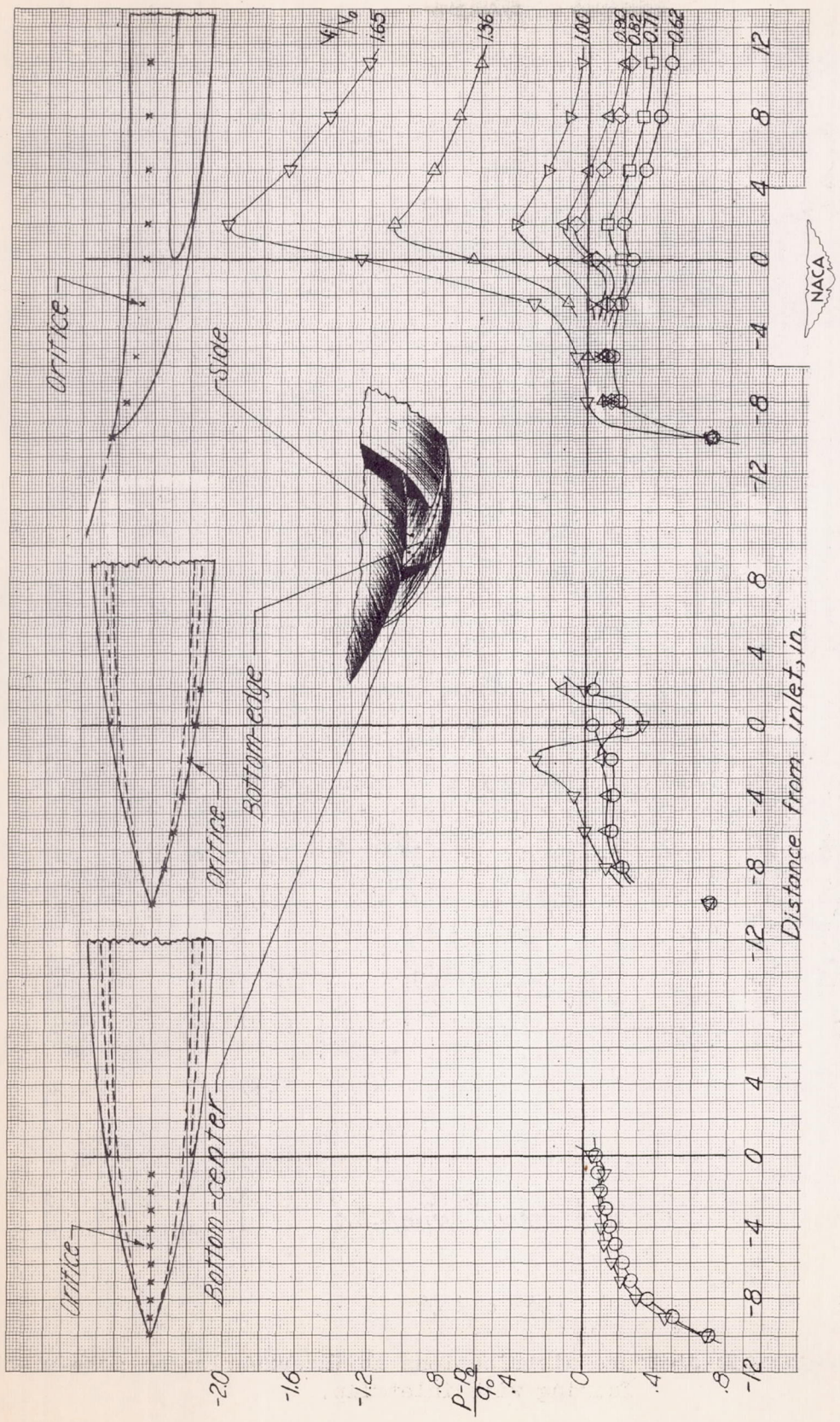

(c) $\alpha = 6^{\circ}$.

Figure 12.- Concluded.

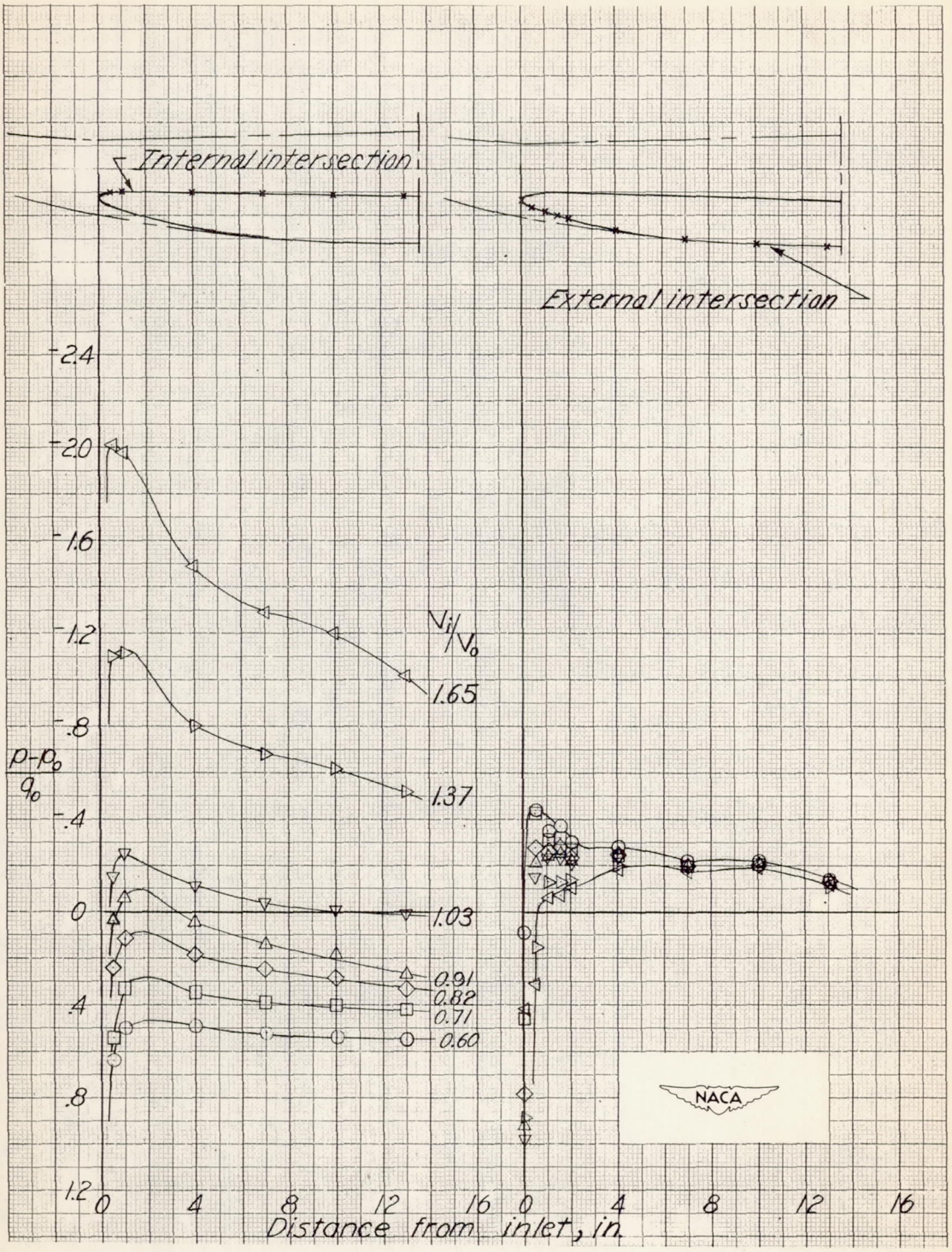

(a) $\alpha = 0^{\circ}$.

Figure 13.- Static-pressure distributions at intersection of nose-wheel fairing with inlet lip.

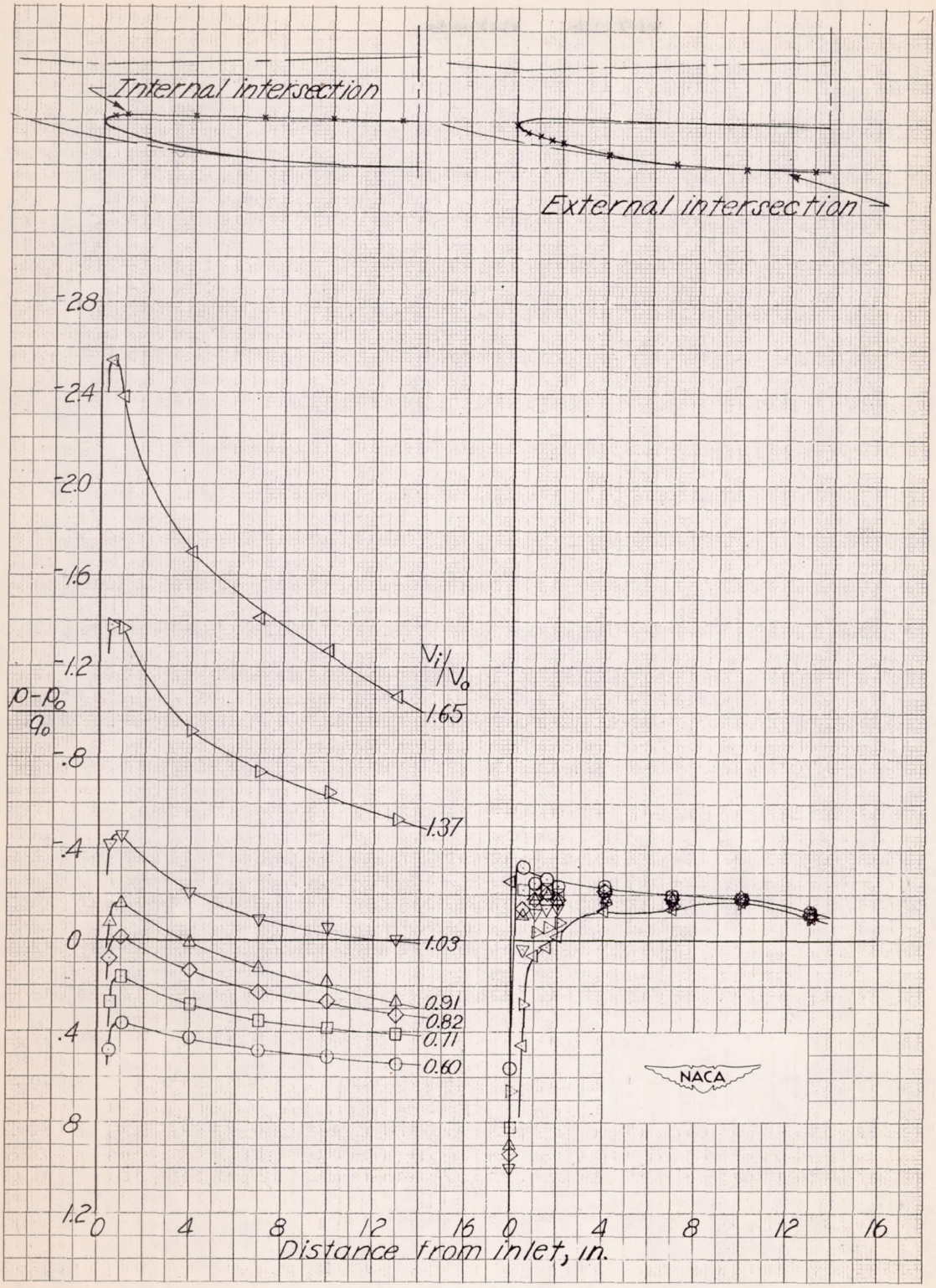

(b) $\alpha = 3^{\circ}$.

Figure 13.- Continued.

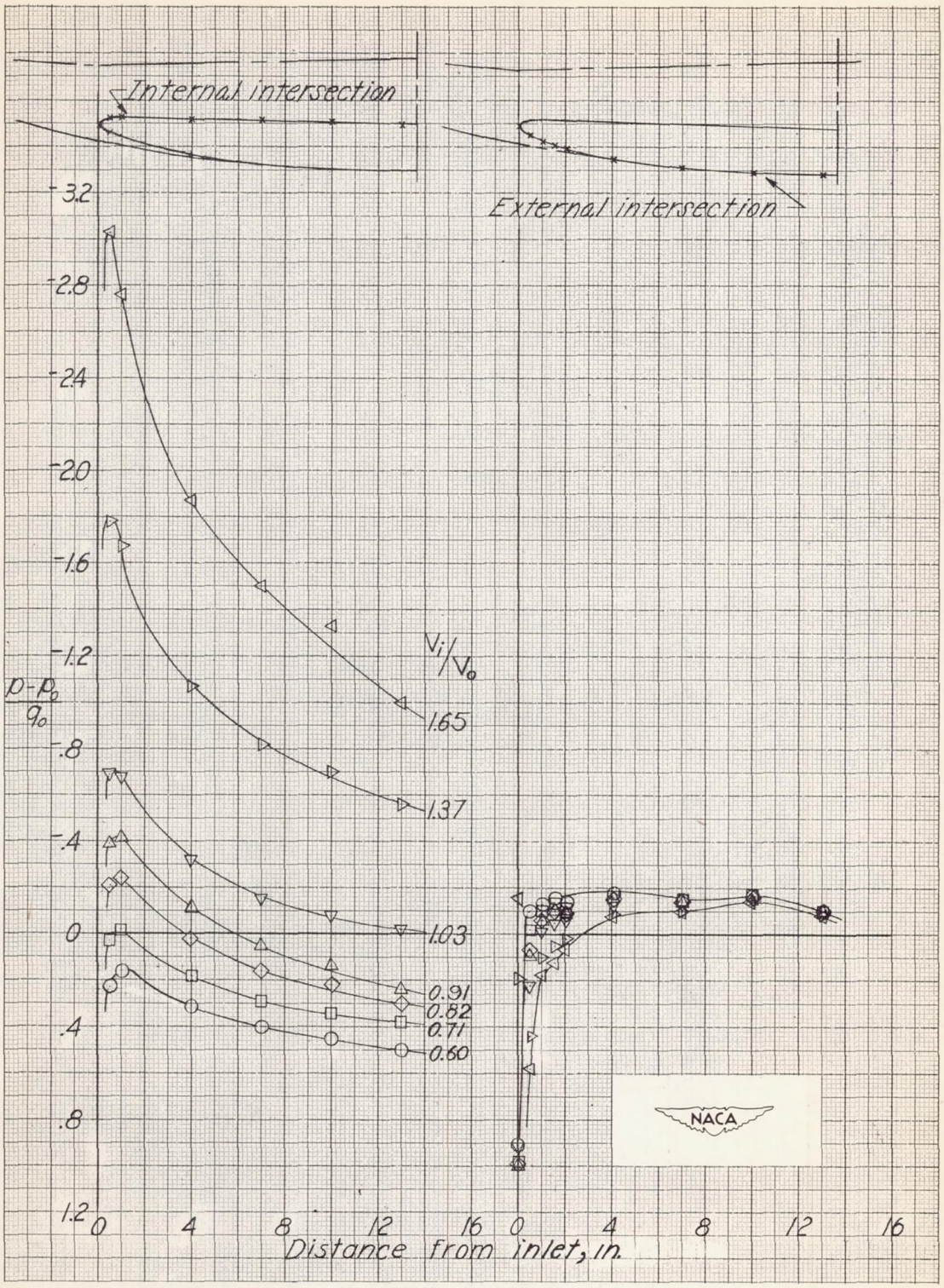

(c) $\alpha = 6^{\circ}$.

Figure 13.- Concluded.

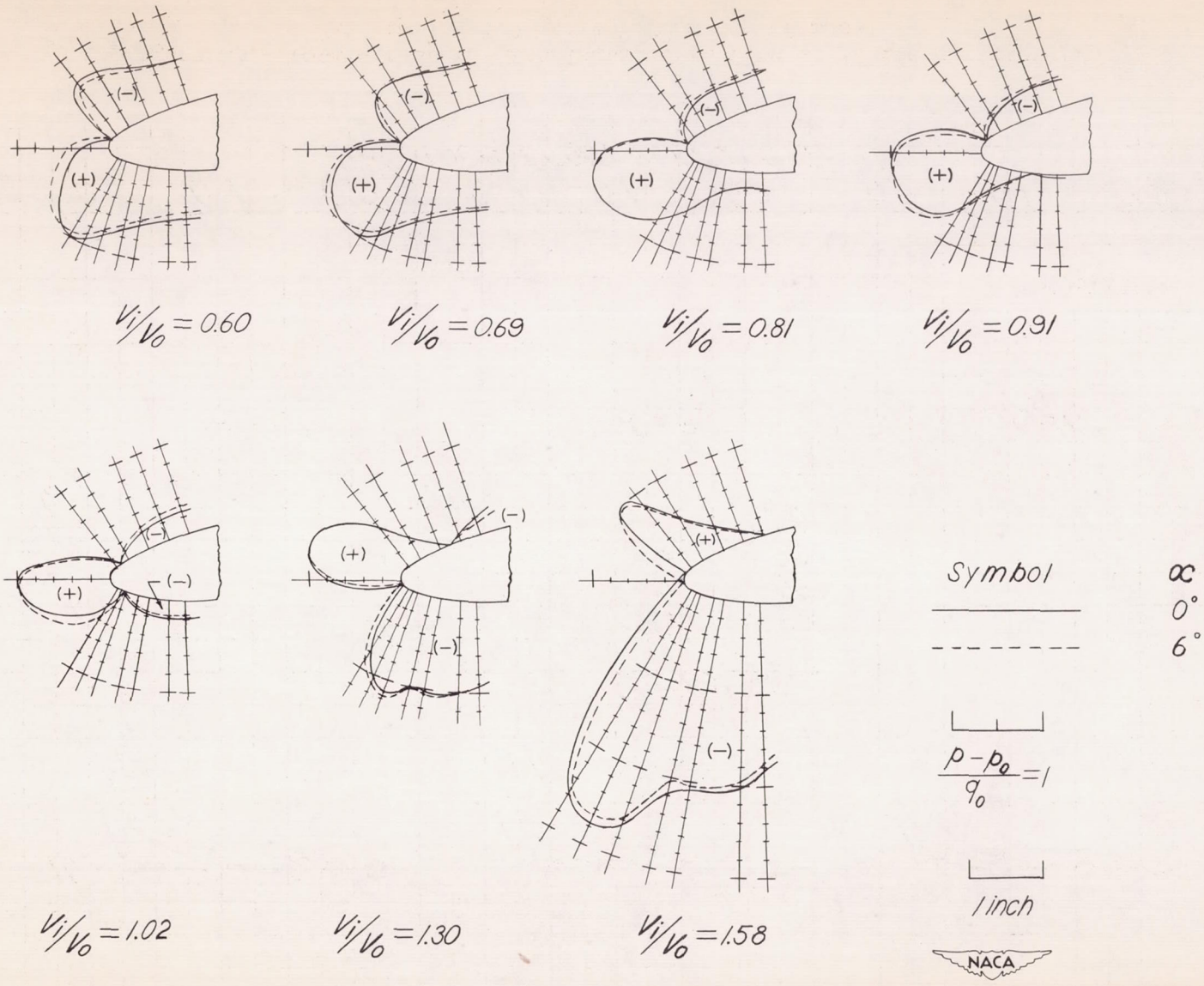

Figure 14.- Static-pressure distributions over inlet lip at horizontal center line of model.

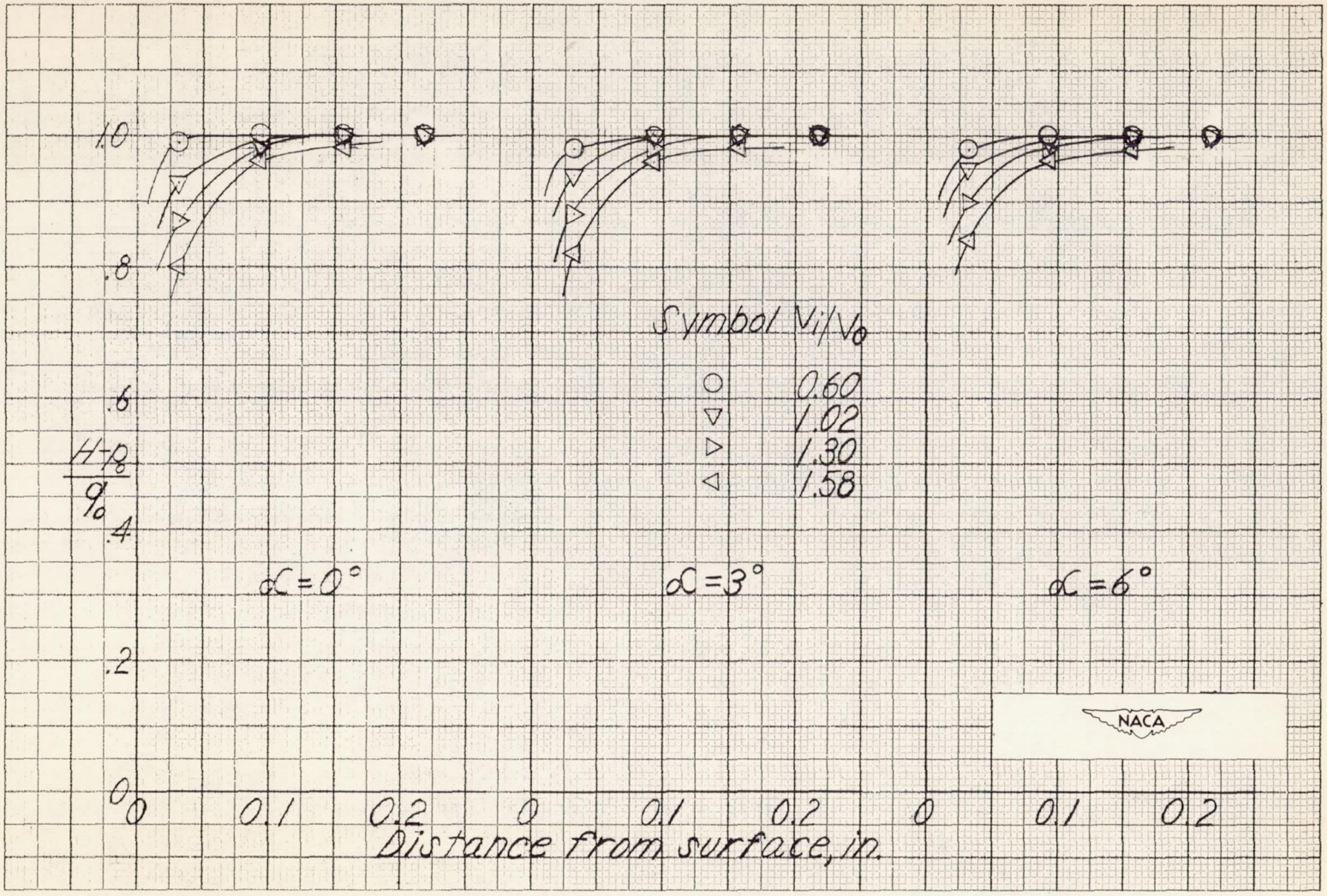

Figure 15.- Total-pressure distributions in flow at inside of inlet lip at station 1.0 and 45° from top of model.

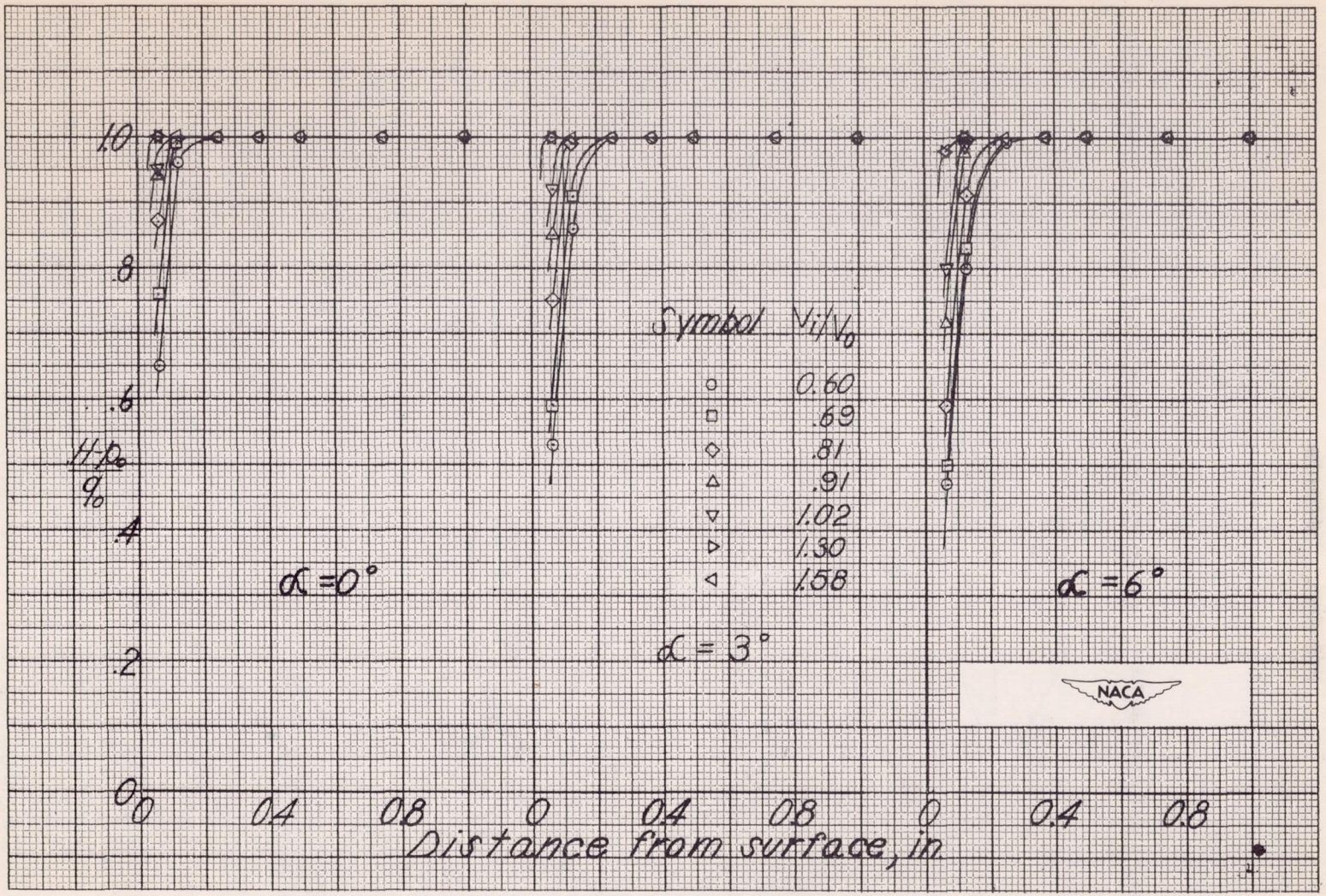

Figure 16.- Total-pressure distributions in external flow on outside of inlet lip at station 12.6 and 45° from top of model.

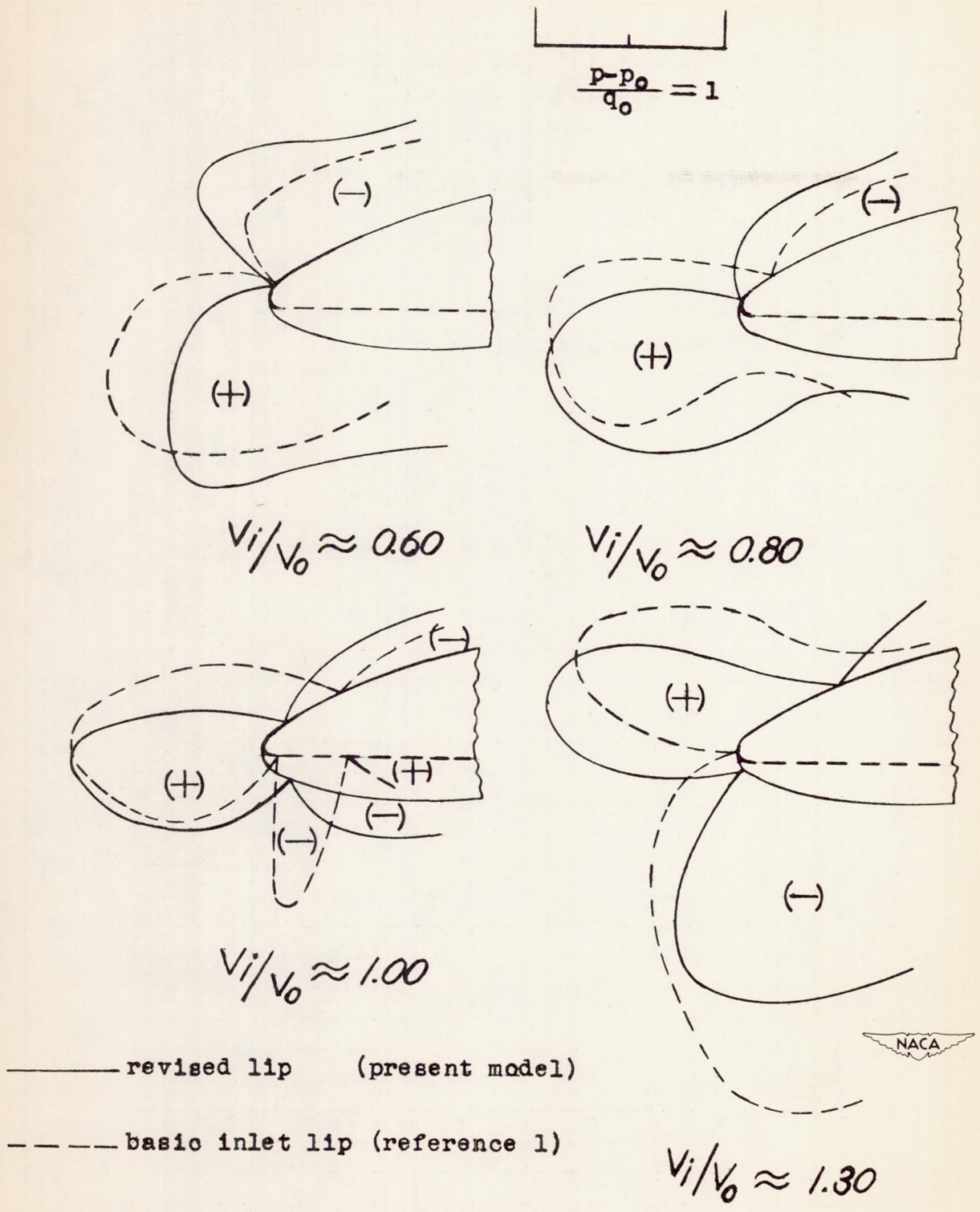

Figure 17.- Effect on pressure distribution of revision to inner fairing of basic inlet lip. $\alpha = 0^{\circ}$.

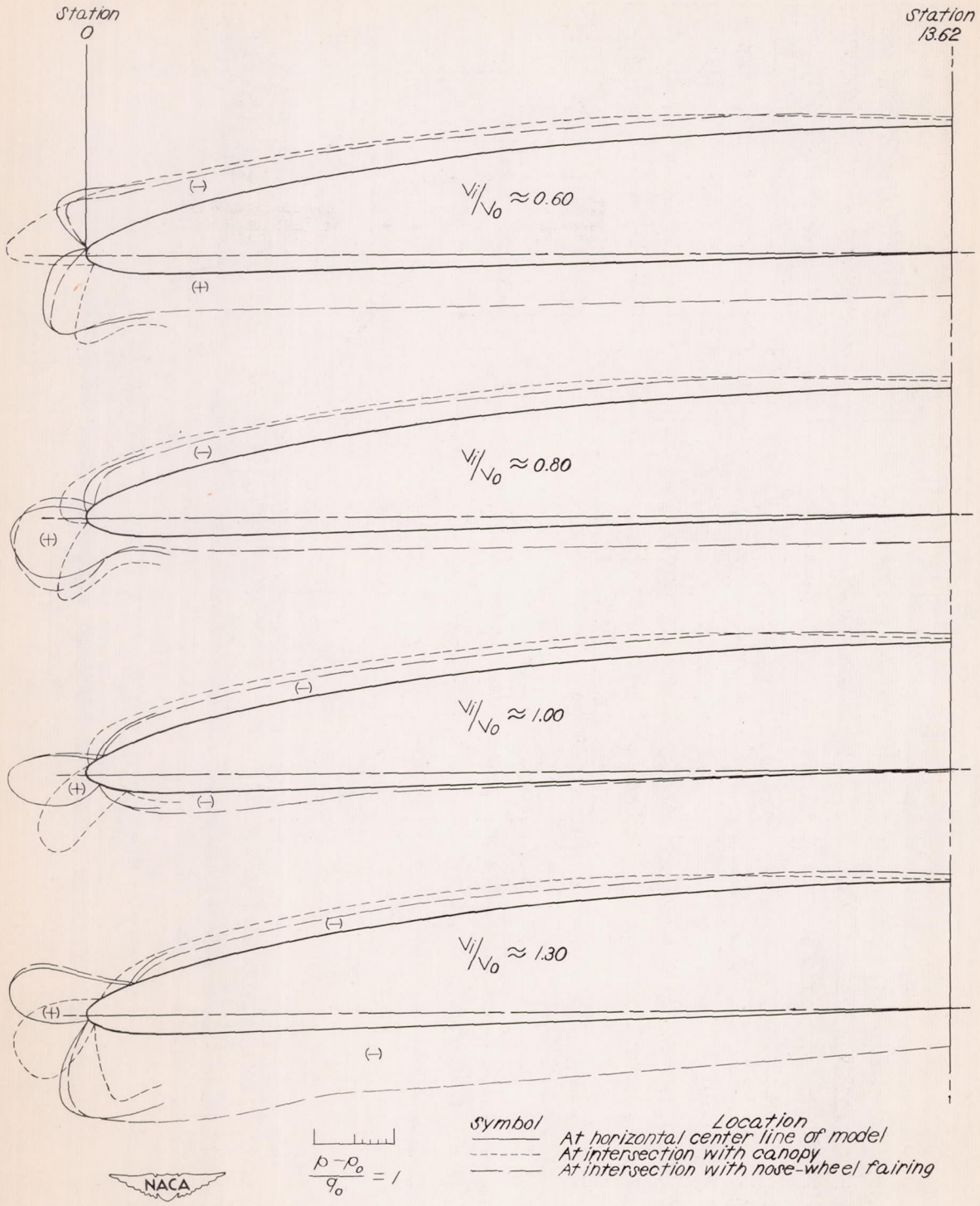

Figure 18.- Comparison of static-pressure distributions over several sections of inlet lip. $\alpha = 0^{\circ}$.

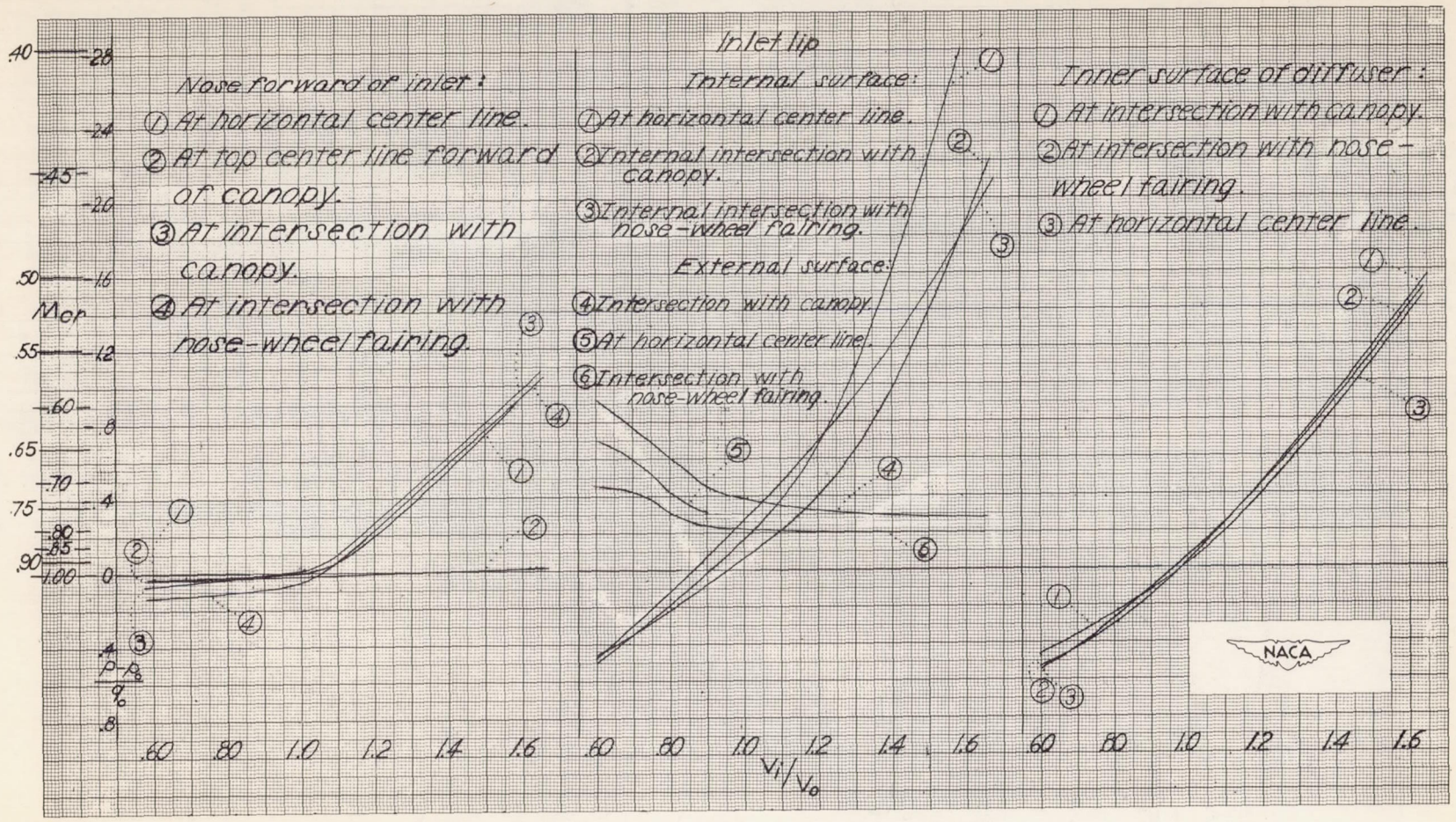

(a) Nose, inlet lip, and inner surface of diffuser.

Figure 19.- Minimum pressures on model components and corresponding predicted critical Mach numbers. $\alpha = 0^\circ$.

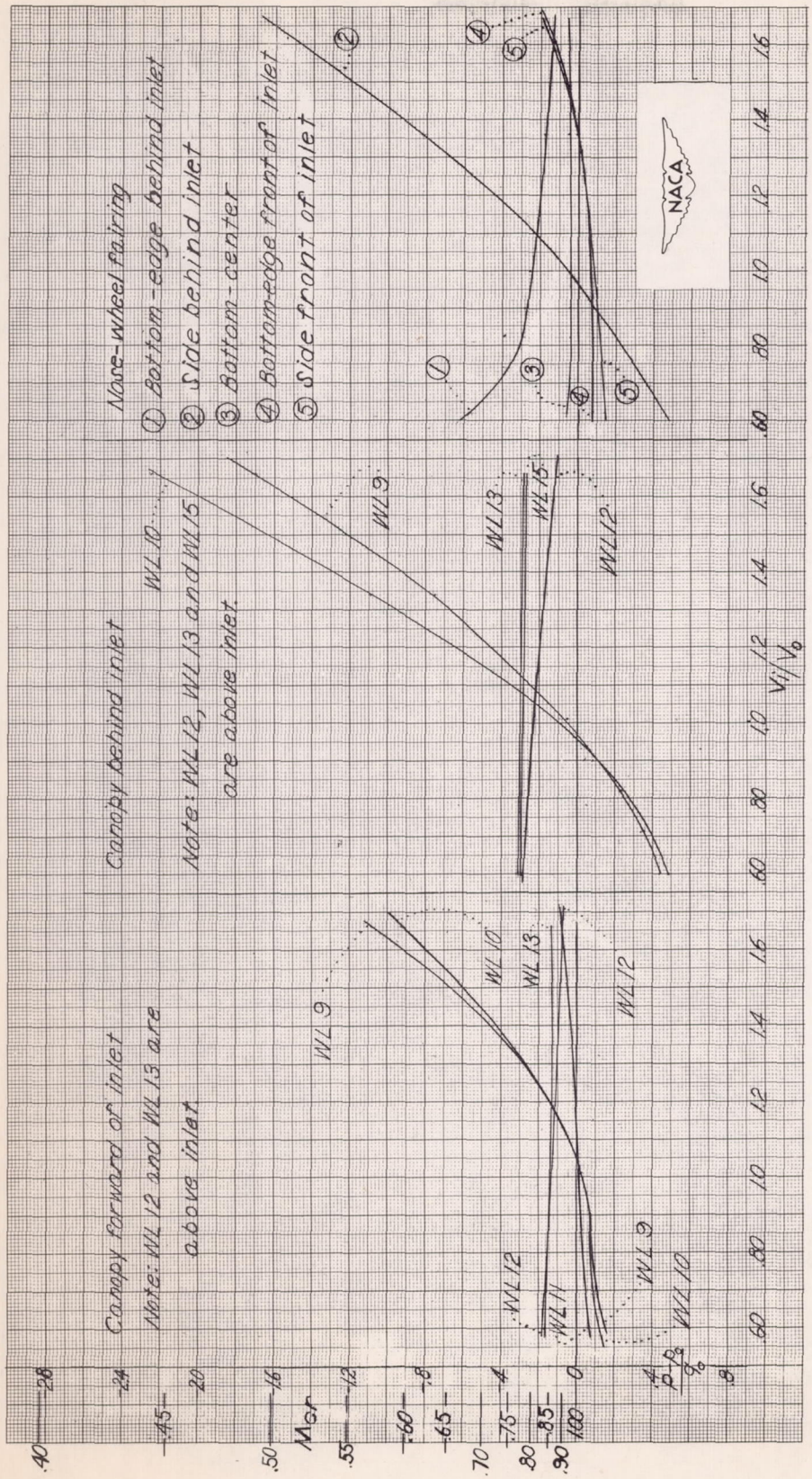

(b) Canopy and nose-wheel fairing.

Figure 19.- Concluded.

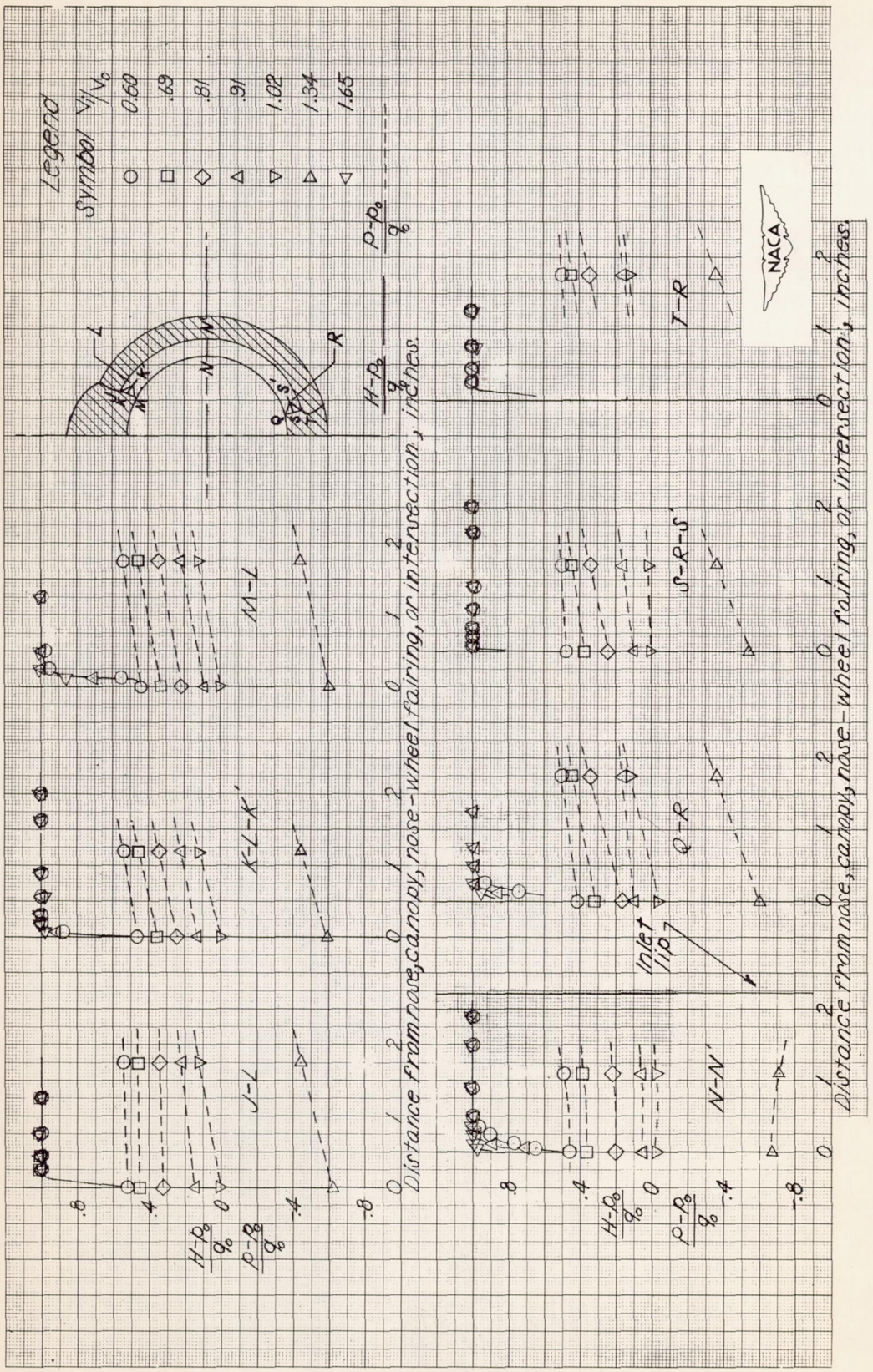

(a) $\alpha = 0^{\circ}$.

Figure 20.- Pressure surveys at inlet. Station 0.3.

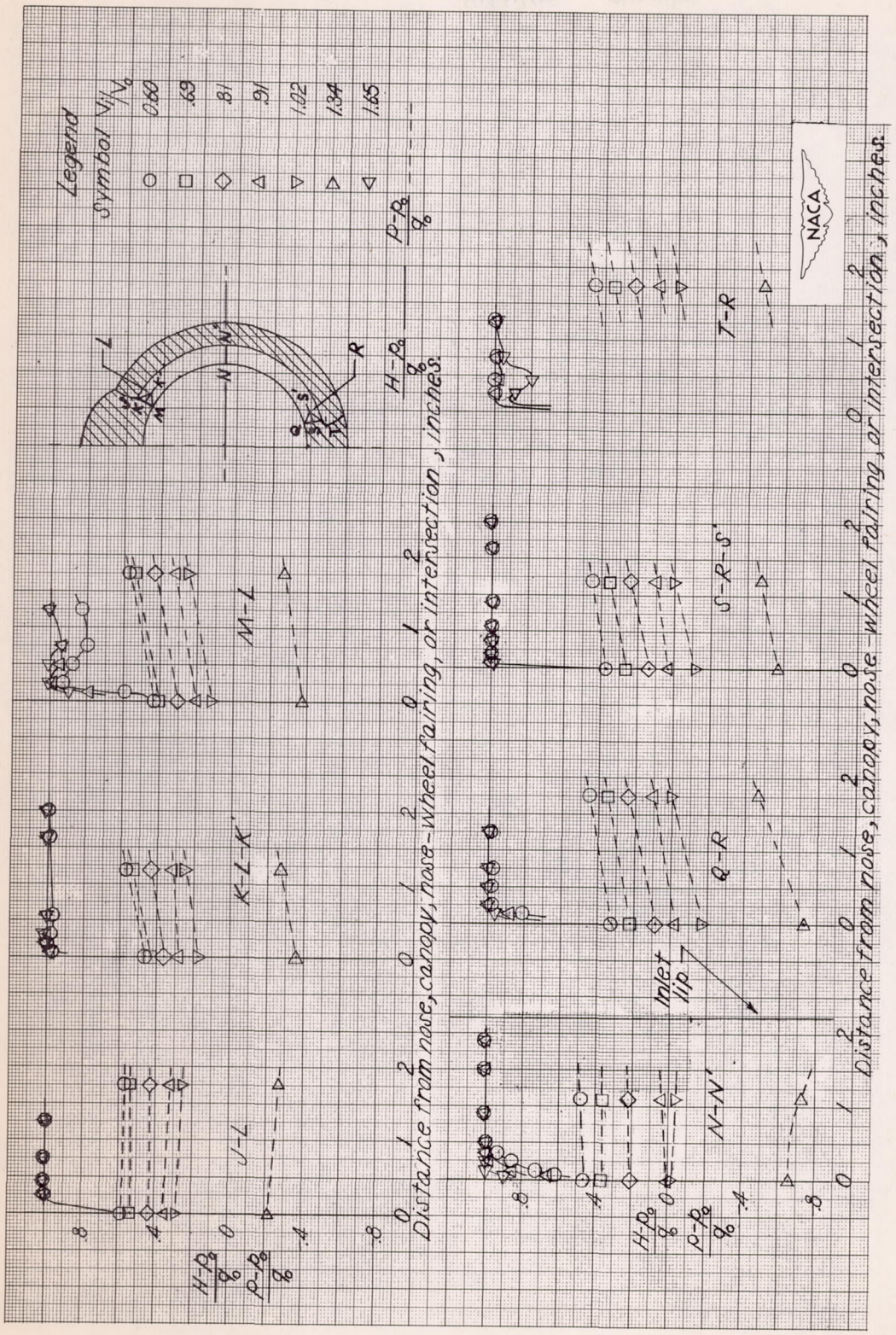

(b) $\alpha = 3^\circ$.

Figure 20.- Continued.

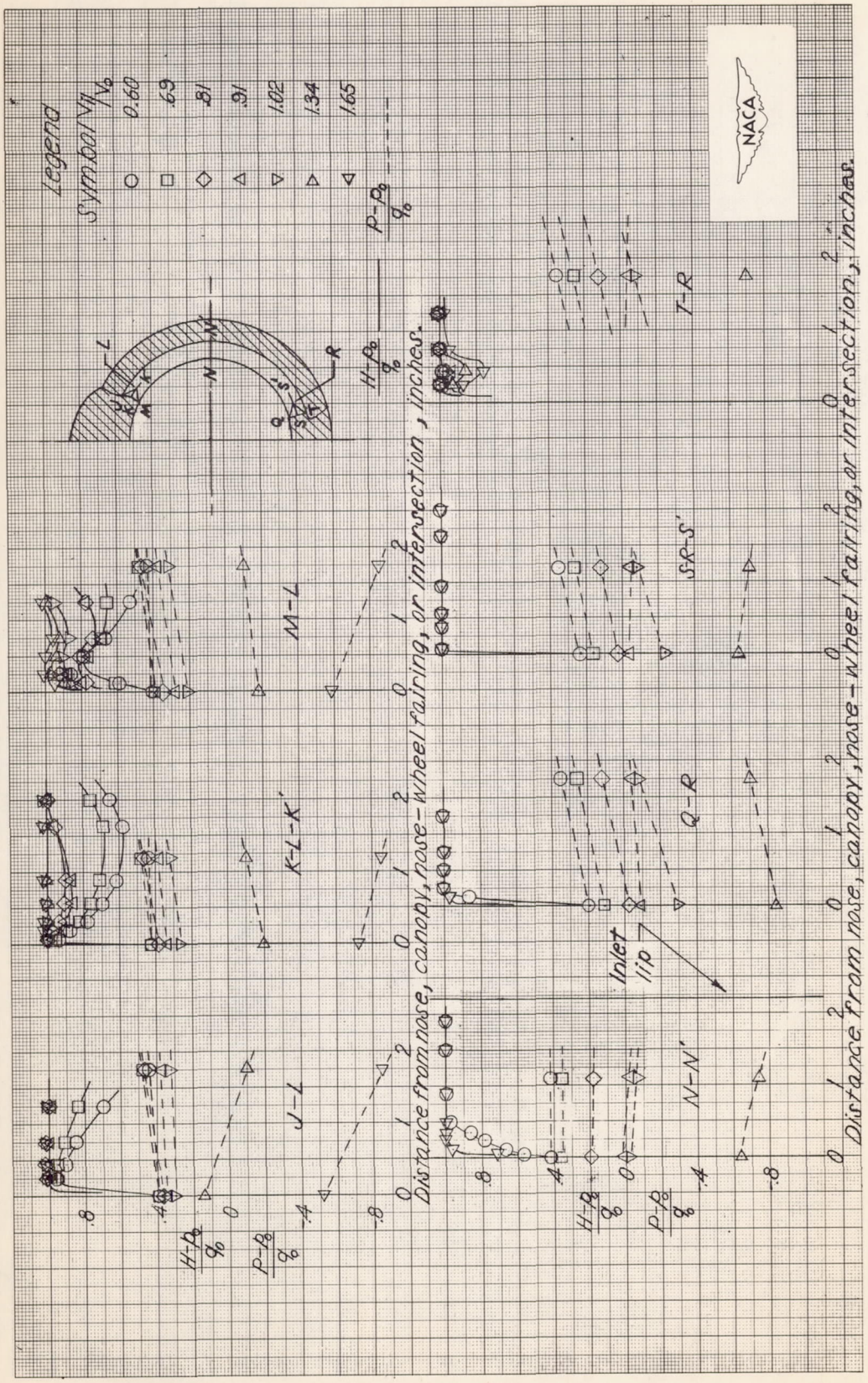

(c) $\alpha = 6^{\circ}$.

Figure 20.- Concluded.

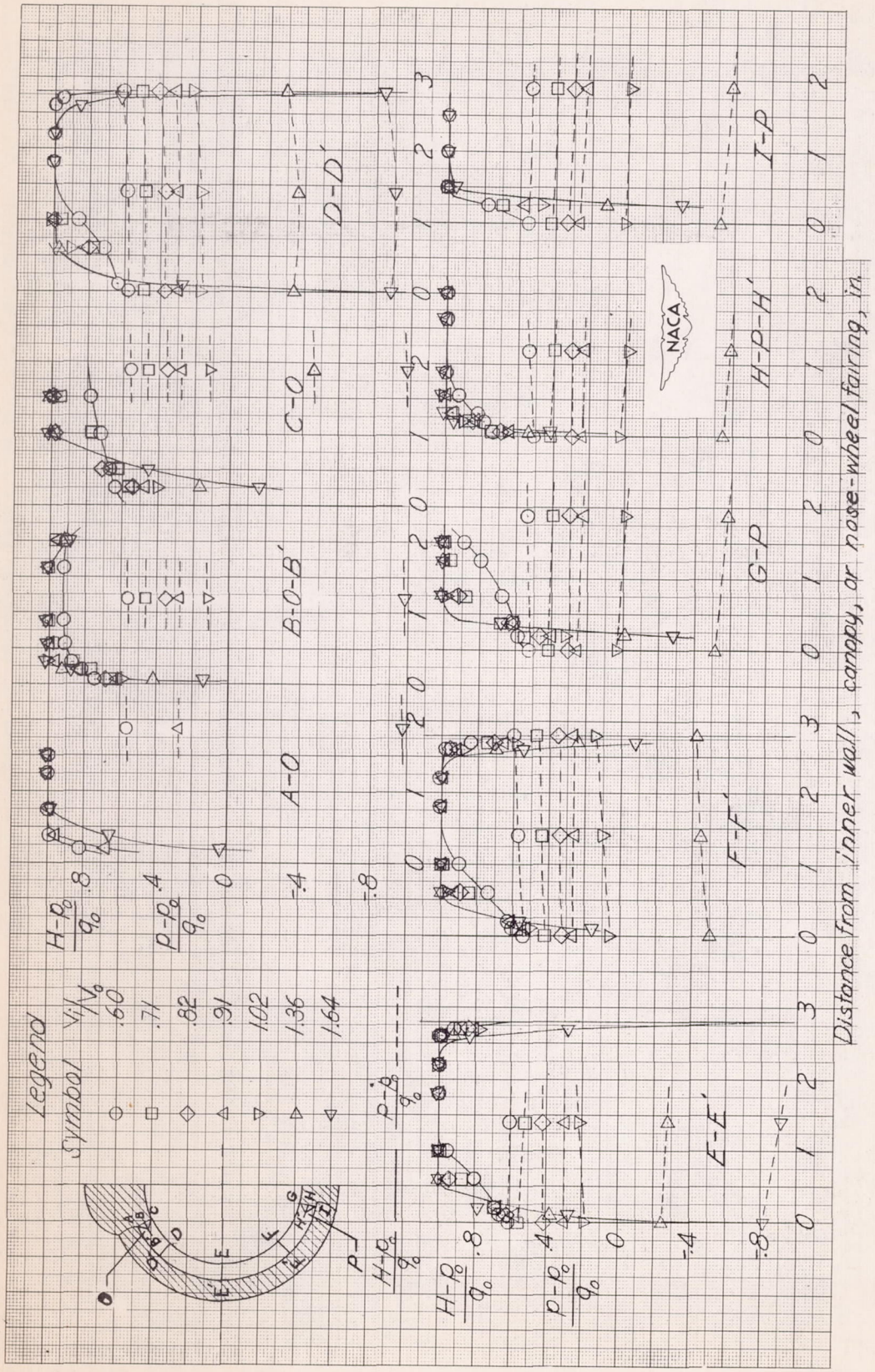

(a) $\alpha = 0°$.

Figure 21.- Pressure surveys in diffuser. Station 12.6.

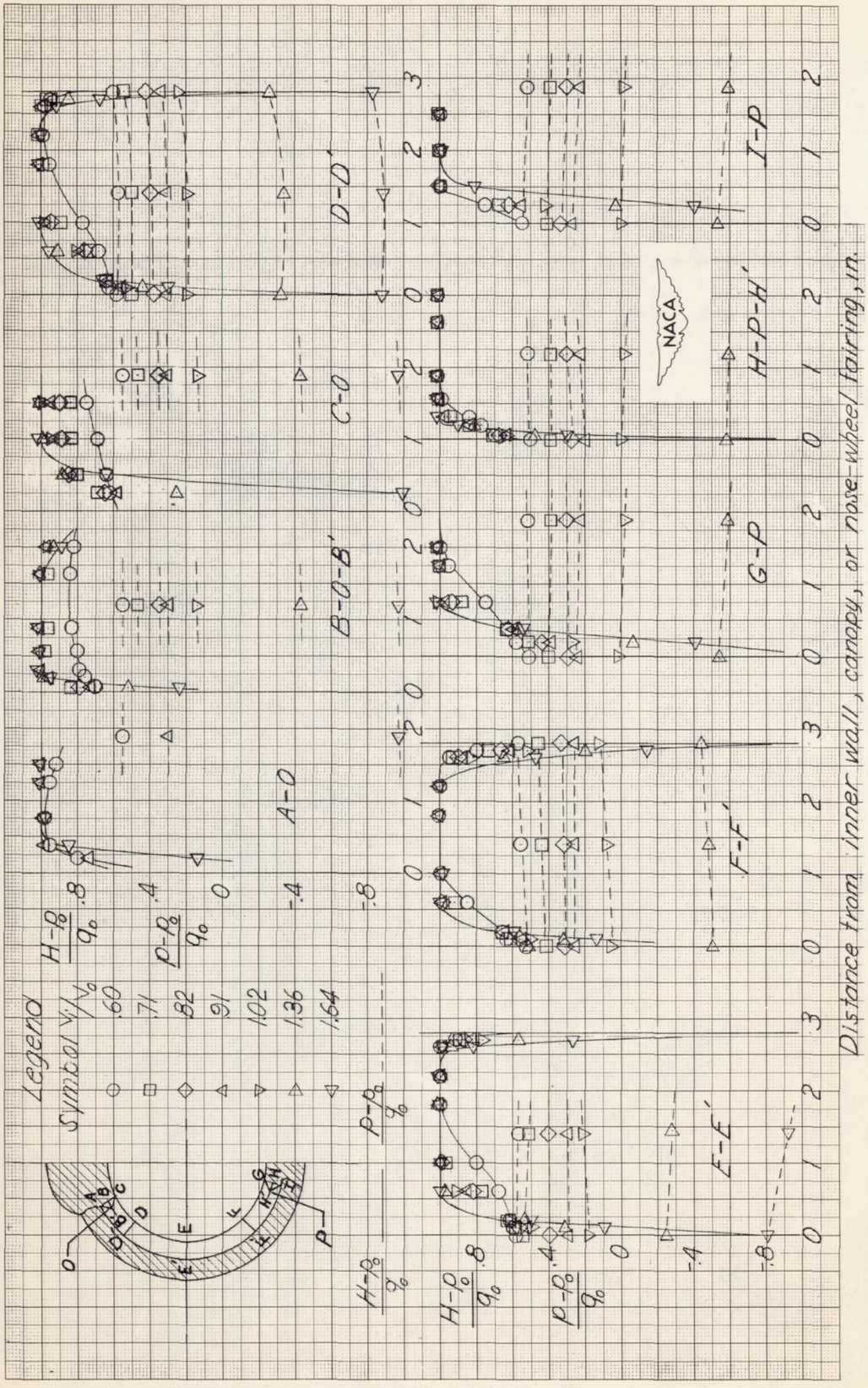

(b) $\alpha = 3^{\circ}$.

Figure 21.- Continued.

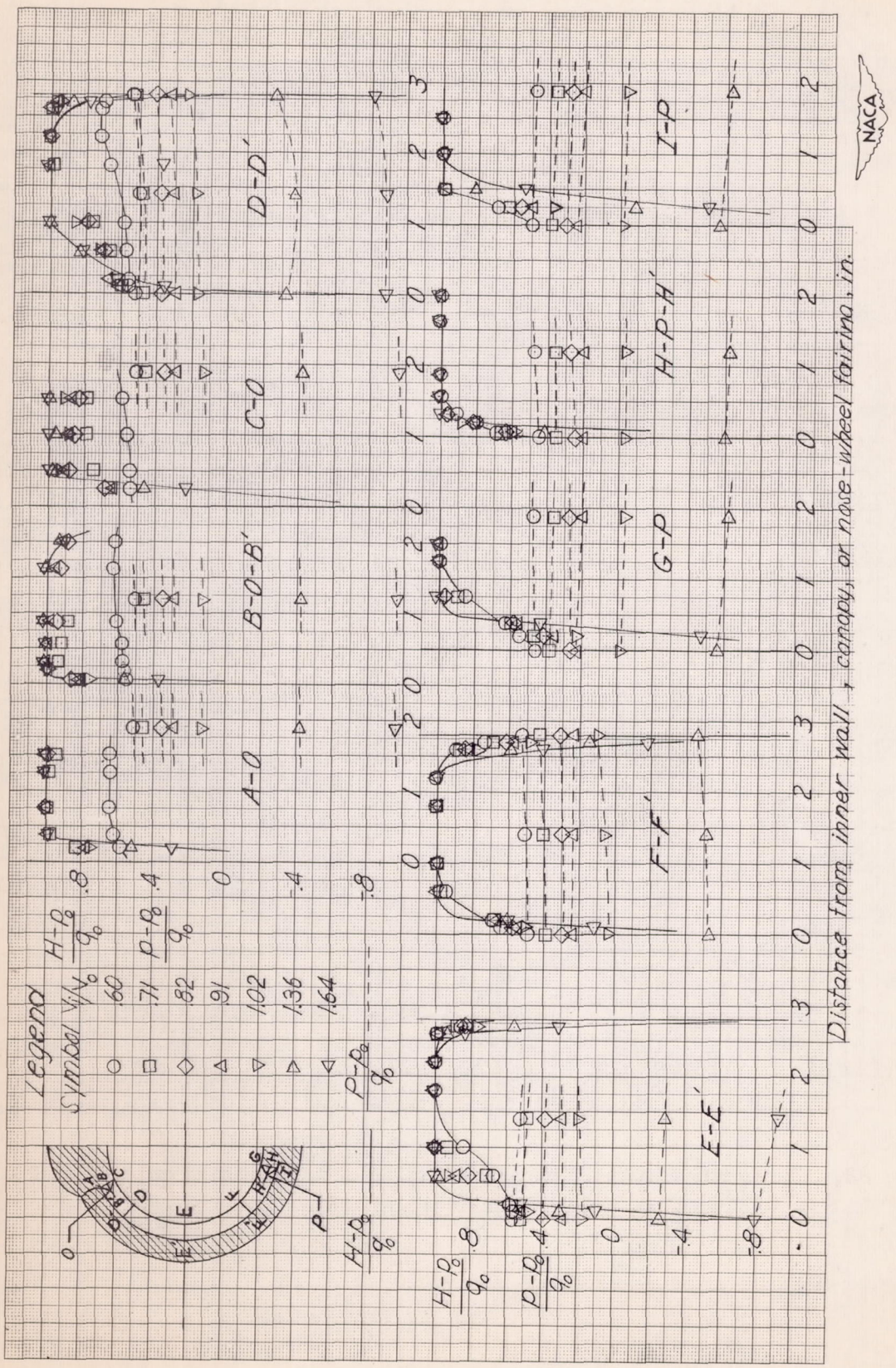

(c) $\alpha = 6^{\circ}$.

Figure 21.- Concluded.

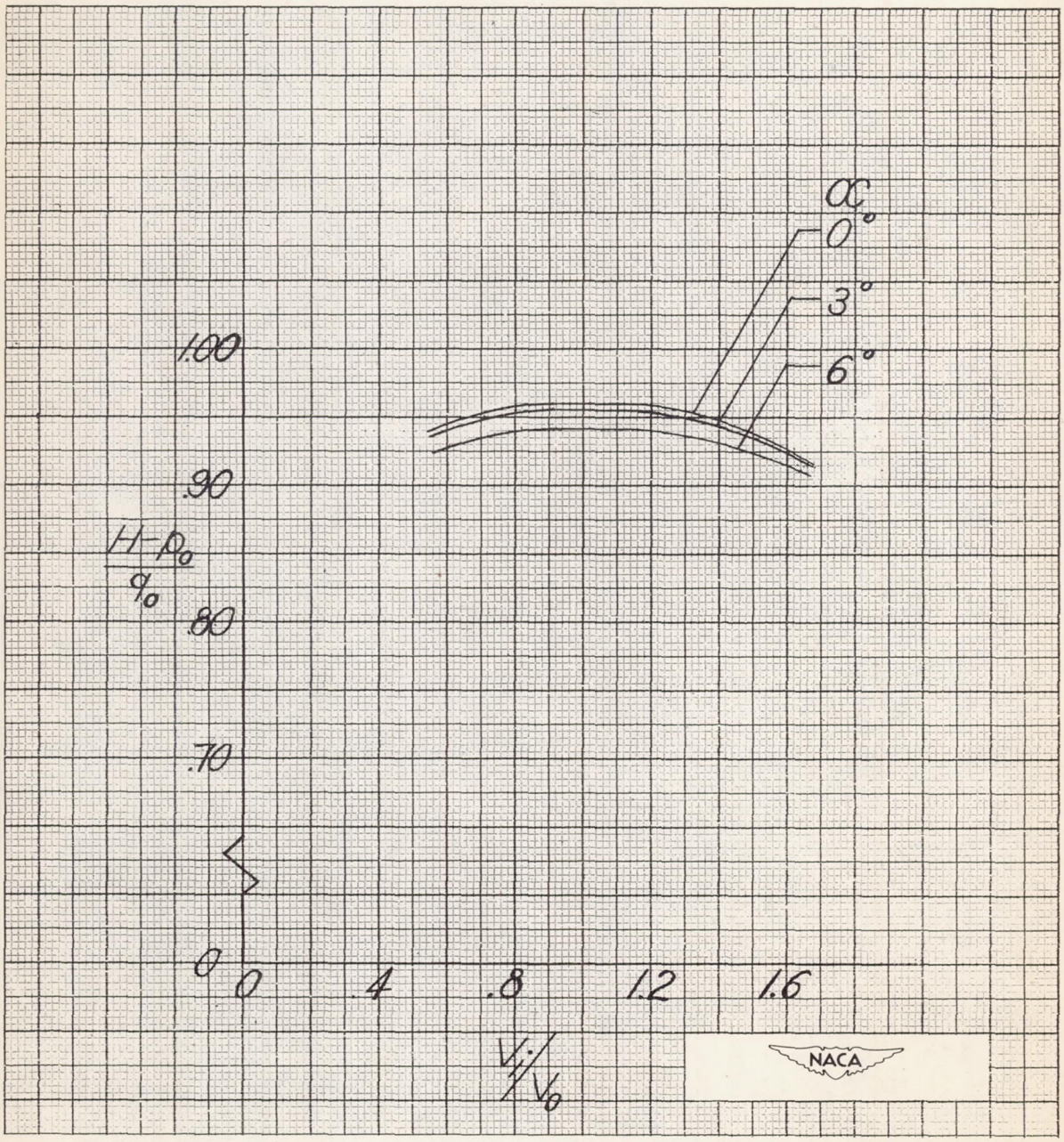

Figure 22.- Integrated average total-pressure recoveries at station 12.6 in diffuser as a function of inlet-velocity ratio.